UNIVERSIDADE D
COIMBRA

Joana Rita Alves Pereira

Investigation of the Excitatory/Inhibitory balance in neurodegenerative movement disorders: a ^{1}H-MRS study

Dissertação no âmbito do Mestrado Integrado em Engenharia Biomédica com especialização em Imagem e Radiação, orientada pelo Professor Doutor Miguel Castelo-Branco e pela Professora Doutora Otília C. d'Almeida e apresentada à Faculdade de Ciências e Tecnologia da Universidade de Coimbra.

Outubro de 2021

UNIVERSIDADE D
COIMBRA

Joana Rita Alves Pereira

Investigation of the Excitatory/Inhibitory balance in neurodegenerative movement disorders: a ^{1}H-MRS study

Thesis submitted to the
University of Coimbra for the degree of
Master in Biomedical Engineering with specialization in
Image and Radiation

Supervisors:
Miguel Castelo-Branco, MD, PhD
Otília C. d'Almeida, PhD

Coimbra, 2021

"Quero, terei;

Se não aqui;

Noutro lugar que ainda não sei.

Nada perdi;

Tudo serei"

Fernando Pessoa

Acknowledgments

Torna-se difícil agradecer a todas as pessoas que contribuíram para que eu estivesse aqui agora a escrever estas palavras, mas vou tentar.

Primeiro, gostava de mostrar a minha gratidão aos meus orientadores, Professora Otília C. d'Almeida e Professor Miguel Castelo-Branco por todo o apoio, incentivos, orientação, elogios e paciência. Foram horas e horas dedicadas a mim. Sem a sua motivação e disponibilidade, ainda agora estava certamente a começar este projeto.

Tenho também que agradecer à minha família, a quem estou muito grata por tudo. A eles, mas em especial a dois amores maiores. À mãe, a minha, por ser a melhor do mundo e aceitar todos os meus devaneios, sempre com paciência e compreensão. Por ser a supermulher que carrega às costas tudo e todos à sua volta! E ao Tomás. Por ser o irmão mais chato do mundo, mas também o mais engraçado, que no meio das suas parvoíces lá me vai ajudando a crescer.

E claro, agradecer aos amigos de uma vida inteira, aos amigos de Coimbra, aos amigos de Erasmus, aos amigos mais antigos e aos amigos mais recentes. Sem estas pessoas à minha volta a incentivar-me e a apoiar-me era tudo bem mais difícil. À Marli, à Jessica, às Marianas (são muitas!), à Marta, à Erica, à Rute, às Margaridas, à Carolina, aos Joãos, ao Alberto, ao Luís, ao Pedro, à Daniela, à Rita, à Mafalda, às Marias, a toda a minha descendência da família de praxe, e a todas e todos que ao longo dos últimos meses me foram aturando e dos últimos anos acompanhando nas minhas aventuras e desventuras.

São estas pessoas que fazem de mim quem sou. Que continuem a manter-se ao meu lado na etapa que a entrega desta dissertação inicia.

Financing

This work was funded by:

Portuguese Foundation for Science and Technology

(MEDPERSYST, ref. POCI-01-0145-FEDER-016428)

CENTRO2020 (BIGDATIMAGE, ref. CENTRO-01-0145-FEDER-000016)

SCML - 'Santa Casa da Misericórdia de Lisboa' (2013 Mantero Belard Neuroscience Prize, 1st edition)

Resumo

As doenças neurodegenerativas incluem várias condições caracterizadas por uma degeneração contínua e acentuada dos neurónios no cérebro. A prevalência dessas doenças tem aumentado em todo o mundo e os tratamentos disponíveis são, na sua maioria, sintomáticos. Portanto, a carga física, emocional e económica para esses doentes e cuidadores é devastadora, enquanto a degeneração vai progredindo nos indivíduos afetados. As doenças neurodegenerativas do movimento, como a Doença de Parkinson (PD) e Huntington (HD), são caracterizadas por graves défices motores, acompanhados de disfunções emocionais e cognitivas. Estas disfunções têm sido relacionadas com alterações no controlo excitatório/inibitório (E/I) pela desconexão progressiva no ciclo gânglios de base-tálamo-cortical. O tónus excitatório e inibitório pode ser avaliado, *in vivo*, por Espectroscopia de Ressonância Magnética de protão (^{1}H-MRS), pois permite estimar indiretamente os níveis de GABA (inibitório) e Glutamato (excitatório).

Portanto, o objetivo deste projeto é estudar o equilíbrio excitatório/inibitório, *in vivo*, no córtex frontal de doentes HD e PD, comparando as razões de Glx (combinação de glutamato e glutamina) e GABA em indivíduos com essas doenças e controlos saudáveis emparelhados para idade e sexo.

Setenta participantes (27 HD; 27 PD; 16 controlos) foram submetidos a um protocolo de Ressonância Magnética a 3T incluindo aquisição de imagens estruturais, funcionais e de espectroscopia. Neste estudo, a análise foi focada em dados de ^{1}H-MRS, adquiridos num voxel de 27mL no lobo pré-frontal. Como o GABA é difícil de resolver no espectro de protão, devido à sua baixa concentração e contaminação do sinal por sinais sobrepostos, foi usada uma abordagem de edição espetral através da sequência de pulso MEGA-PRESS. O processamento de dados espectrais foi realizado usando o Gannet e a análise estatística foi realizada no software estatístico R. Um doente de Huntington foi excluído, pois os dados de MRS não foram adquiridos na mesma região anatómica.

Após uma avaliação visual inicial de controlo de qualidade dos espectros, 44 conjuntos de dados foram descartados. A nossa hipótese é que o movimento excessivo, ao qual a MRS é particularmente sensível, foi o artefato predominante que contribuiu para a alta taxa de rejeição. No entanto, vários fatores que afetam a qualidade do sinal podem ser considerados: permanecer completamente imóvel é um desafio para doentes com PD e HD em neuroimagem; o movimento leva ao deslocamento do voxel causando artefatos de contaminação por volumes parciais; o lobo frontal é uma área particularmente sensível para aquisição de MRS devido a artefatos de suscetibilidade; realizar ^{1}H-MRS após fMRI pode produzir desvios de frequência devido aos gradientes aplicados; etc. Encontramos algumas tendências nos níveis de GABA e Glx entre os grupos, mas não foram estatisticamente significativas e os resultados são inconclusivos.

Um debate sobre as medidas de avaliação de qualidade e métodos recentes de correção de artefatos foi brevemente realizado. Estudos futuros de ^{1}H-MRS focando em populações especiais propensas ao movimento, como populações clínicas, e também em recém-nascidos e crianças pequenas devem ter um desenho de estudo e plano de análise de dados ainda mais criteriosos, tendo em consideração as taxas de exclusão de dados devido aos critérios de garantia de qualidade, o protocolo de aquisição e algoritmos de processamento de dados.

Palavras-Chave: Espetroscopia por Ressonância Magnética, Doença de Huntington, Doença de Parkinson, GABA, Técnica de edição espetral

Abstract

Neurodegenerative diseases span several conditions characterized by a continuous and massive neural degeneration in distinct brain regions. The prevalence of these disorders is rising worldwide, and the available treatments are mostly symptomatic. Therefore, the physical, emotional, and economic burden to these patients and caregivers is devastating while degeneration progresses in the afflicted individuals. Neurodegenerative movement disorders, such as Parkinson's (PD) and Huntington's Disease (HD) are characterized by severe motor deficits accompanied with emotional and cognitive dysfunctions. These dysfunctions have been related with alterations on excitatory/inhibitory (E/I) control with a progressive disconnection in basal ganglia-thalamocortical loops. Excitatory and inhibitory tonus may be evaluated, *in vivo*, using proton Magnetic Resonance Spectroscopy (^{1}H-MRS) since it allows to indirectly estimate GABA (inhibitory) and Glutamate (excitatory) levels.

Therefore, the objective of this project is to study the Excitatory/Inhibitory balance, *in vivo*, in the frontal cortex of HD and PD patients by comparing Glx (pool of glutamate and glutamine) to GABA ratios between these clinical disorders with healthy age- and gender-adjusted Control participants.

Seventy participants (27 HD; 27 PD; 16 Controls) were submitted to a 3T MRI protocol including structural, functional and spectroscopic imaging. In this study, analysis was focused on ^{1}H-MRS data, acquired in a 27mL voxel in the prefrontal lobe. Since GABA is difficult to resolve in the proton spectra, due to its low concentration and signal contamination by overlapping signals, a J-difference editing approach was used with MEGA-PRESS pulse sequence. Spectral data processing was performed using Gannet and statistical analysis was performed using R statistical software. One HD patient was excluded since MRS data was not acquired in the same anatomical region.

After an initial visual quality control assessment of the spectra, 44 datasets were discarded. We do hypothesize that excessive motion, to which MRS is particularly

sensitive, was the predominant artifact contributing for the high rate of dropouts. Nonetheless several factors affecting the signal quality may be considered: staying completely still is a challenge for neuroimaging PD and HD patients; motion leads to voxel misplacement and partial volume artifacts; the frontal lobe is a particularly sensitive area for MRS acquisition due to susceptibility artifacts; performing the ^{1}H-MRS after fMRI may produce frequency drifts due to the applied gradients; etc. We found some trends on GABA and Glx levels between groups, yet these were not statistically significant, and results are thus inconclusive.

A discussion on the quality assurance measures, which are often absent in the literature, and recent artifacts correction methods was briefly performed. Future ^{1}H-MRS studies focusing special populations prone to movement such as clinical patients, and also infants and small children must have an even more thorough study design and data analysis plan, accounting for dropout rates due to quality assurance criteria, the acquisition protocol, and data processing algorithms.

Keywords: Magnetic Resonance Spectroscopy, Huntington's Disease, Parkinson's Disease, GABA, J-difference editing technique

List of Acronyms

B_0 Main Magnetic Field.
BH Benjamini-Hochberg Correction.

Cho Choline.
CPNs Cortical Pyramidal Neurons.
Cr Creatine.
CRMVB Cramer-Rao Minimum Variance Bounds.
CSF Cerebrospinal Fluid.
CSI Chemical Shift Imaging.

DBS Deep Brain Stimulation.

E/I Excitatory/Inhibitory Balance.

FA Flip Angle.
FFT Fast Fourier Transform.
fMRI Functional Magnetic Resonance Imaging.
FoV Field of View.
FWHM Full Width at Half Maximum.

GABA γ -aminobutyric acid.
Gln Glutamine.
Glu Glutamate.
Glx Pool of glutamate and glutamine.
GM Gray Matter.
GPC Glycerophosphocholine.
GPe Globus Pallidus External.
GPi Globus Pallidus Internal.

HD Huntington's Disease.
HERMES Hadamard Encoding and Reconstruction of MEGA-Edited Spectroscopy.
HTT Huntingtin.

Ins Myo-inositol.

Lac Lactate.
LASER Localization by Adiabatic Selective Refocusing.
L-DOPA Levodopa.

MEGA-PRESS MEscher-GArwood Point Resolved SpectroScopy.
MPRAGE Magnetization Prepared Rapid Acquisition Gradient Echo.
MR Magnetic Resonance.
MRI Magnetic Resonance Imaging.
MRS Magnetic Resonance Spectroscopy.
MRSI Magnetic Resonance Spectroscopic Imaging.

NAA N-acetylaspartate.
NAAG N-acetylaspartylglutamate.
NMR Nuclear Magnetic Resonance.
NWS No Water Suppression.

PC Phosphocholine.
PCr Phosphocreatine.
PD Parkinson's Disease.
PET Positron Emission Tomography.
ppm Parts per milion.
PRESS Point REsolved SpectroScopy.

RF Radiofrequency.

SNc Substantia Nigra *pars* Compacta.
SNr Substantia Nigra *pars* Reticulata.
SNR Signal-to-noise Ratio.
SPNs Spiny Projection Neurons.
STEAM STimulated Echo Acquisition Mode.
STN Subthalamic Nucleus.
SVS Single Voxel Spectroscopy.

tDCS Transcranial Direct Current Stimulation.
TE Echo Time.
TMS Transcranial Magnetic Stimulation.
TR Repetition Time.

VOI Volume of Interest.

WM White Matter.

List of Figures

List of Tables

Contents

1

Introduction

1.1 Neurodegenerative Diseases

Neurodegenerative diseases encompass a group of distinct disorders characterized by a chronic degeneration of brain structures, and concomitant impact on its function and physiology. Movement disorders such as Parkinson's Disease (PD) and Huntington's Disease (HD) are part of this heterogeneous group of disorders which prevalence has been increasing in the past decades. Characterized by severe motor deficits, these diseases are often accompanied by concomitant emotional and cognitive dysfunctions and have been related with alterations of inhibitory control in the basal ganglia and thalamocortical circuitry.

1.1.1 Neurodegenerative movement disorders: PARKINSON'S DISEASE

Parkinson's Disease is a common neurodegenerative disease among elderly populations (aged 65+) [1]. Otherwise rare before the age of 50, and in many cases with a genetic basis for onsets before that age, its incidence increases in each subsequent decade, making aging the greatest risk factor for PD. It is estimated that every year there are 5 to 35 (per 100.000 inhabitants) new cases worldwide and that costs associated with PD will rise, because health care has improved and thus allowing for longer survival of individuals in general [1].

Although not fully understood, the pathophysiology of PD has been associated with a preferential loss and/or impairment of dopaminergic neurons in specific areas of the substantia nigra, which leads to a depletion of dopamine in the putamen [2] and an accumulation of α-synuclein aggregates in neurons [1]. Dopamine is responsible for sending modulatory signals to brain regions that control movement and coordination

[3] among many other functions.

PD symptoms are mostly motor but can also be non-motor (Table 1.1). The most common motor symptoms include tremor, bradykinesia, rigidity, postural deformities and instability and freezing/motor blocks [4, 5]. Non-motor symptoms, which tend to precede the motor [1], include cognitive impairment, autonomic dysfunction, sleep disorders as well as anxiety, depression, or apathy, among others [1, 4, 5].

Table 1.1: Most common Parkinson's Disease motor and non-motor symptoms [1, 4, 5].

Motor Symptoms	Non-motor Symptoms
tremor	cognitive impairment
bradykinesia	autonomic dysfunction
rigidity	sleep disorders
postural deformities and instability	depression and anxiety
freezing/motor blocks	apathy

There is still no cure for this disease, meaning that ultimately patients will suffer from a severe progressive disability. Yet symptomatologic dopaminergic therapies are available, the main being levodopa (L-DOPA) [4,6], a precursor of dopamine, in order to improve patients' quality of life [1]. L-DOPA, unlike dopamine, can pass the blood-brain-barrier in the brain and there it can change into dopamine [3]. However, in long-term, these therapies are not sustainable due to the rise of treatment-resistant motor problems [6]. More recently Deep Brain Stimulation (DBS) has also been suggested as a potential tremor alleviation therapy [1, 4], as well as Transcranial Direct Current Stimulation (tDCS) and Transcranial Magnetic Stimulation (TMS) that were also shown to be beneficial in improving motor signs in patients suffering with this disease [7, 8].

Some studies were able to demonstrate molecular changes in the striatum in people with PD before they were even diagnosed [1] and the progression of the disease was linked to a process affecting the dorsal putamen in earlier stages and the ventral putamen with increasing disease severity in a study that used coregistration of Positron Emission Tomography ([^{18}F-dopa]-PET) and MRI images [9].

1.1.2 Neurodegenerative movement disorders: HUNTINGTON'S DISEASE

In 1872, George Huntington described a chronic progressive neurodegenerative disorder involving the degeneration of neurons in the basal ganglia [2] that affected both movement and cognition as well as personality [10]. Only one century after Huntington's first description of the disease, in 1993, the responsible gene was discovered [11]. Since then, with the advances of brain imaging techniques many theories for the pathogenesis have been proposed and studied. The discovery of the responsible gene led to earlier diagnosis and promoted the development of new symptomatic treatments [11, 12] aiming to ameliorate the quality of life of these patients.

HD is a rare genetic condition [11] caused by an autosomal dominant mutation of the huntingtin (HTT) gene on chromosome 4, affecting about 1 in 10.000 people worldwide [13]. It has an autosomal dominant inheritance meaning that the disorder is developed with a single copy of the defective gene.

This disease involves degeneration of neurons in the basal ganglia, the striatum being particularly susceptible, and which atrophy is associated with the loss of GABAergic (GABA, γ -aminobutyric acid) neurons [13]. Changes in neuronal function, such as increased cortical excitability and decreased GABA-mediated cortical inhibition arise before noticeable cell death, suggesting that circuitry alterations trigger the early symptoms of patients with this disease [13].

It is estimated that symptoms such as involuntary movements (motor disturbances), dementia (cognitive disturbances) and depression, anxiety, and apathy (psychiatric disturbances), as well as less prevalent others (Table 1.2), affect around 5 to 10 per 100.000 people in the Caucasian population [11, 14]. HD mostly manifests between 30 and 50 years, and life expectancy is around 17 to 20 years after the diagnosis. With the course of the disease, patients progressively become more dependent to execute their daily tasks consequent of a quick cognitive and physical capacities deterioration [11].

Table 1.2: Most common Huntington's Disease motor and non-motor symptoms [11, 14, 15].

Motor Symptoms	Non-motor Symptoms
involuntary movements	dementia
incoordination	executive dysfunction
rigidity	depression
mobility disorders	anxiety
speech/swallowing difficulties	apathy

1.1.3 Movement disorders affected circuitries and alterations of inhibitory control

Movement disorders are characterized by complex changes in information processing as, for example, abnormal neural synchronization and cortico-subcortical coupling in specific frequency bands [1].

The basal ganglia take part in several parallel, yet anatomically segregated, cortico-basal ganglia-thalamo-cortical loop. The characteristic circuits from basal ganglia have important functions in the control of actions and goal-oriented behavior. There are four circuits that have a similar functional organization that subserve, among others, motor functions. They do this by linking the corresponding frontal cortical areas and subregions of thalamus and basal ganglia [1] (Figure 1.1).

In PD, there is a decrease in dopaminergic transmission in the motor region of the striatum (in which caudate nucleus and putamen are included) with divergent effects on the direct and indirect pathways that results in increased GABAergic inhibition of thalamo-cortical projections [1]. This indicates that symptoms such as akinesia are physiological consequences of increased inhibitory output activity of the basal ganglia, rather than just occurring due to a "loss of function" [1, 16]. In people with Parkinson, there is a breakdown of the frontal lobe inhibitory mechanisms, which explains the reemergence of primitive reflexes [4].

Basal ganglia are also one of the most vulnerable regions of HD, along with the neocortex [13]. In the neocortex it is possible to find cortical pyramidal neurons (CPNs) and interneurons. CPNs are excitatory glutamatergic neurons whereas interneurons are inhibitory GABAergic cells [13]. Most of the glutamatergic innervation from CPNs directs to the striatum, which is part of the basal ganglia. Even though it receives afferents from all cortical areas, we will be focusing on the motor circuitry, one of the most relevant affected systems in HD [13].

GABAergic spiny projection neurons (SPNs) are the most numerous neurons in the striatum and are subdivided into two types that origin the two main striatal projections: direct and indirect pathways [13].

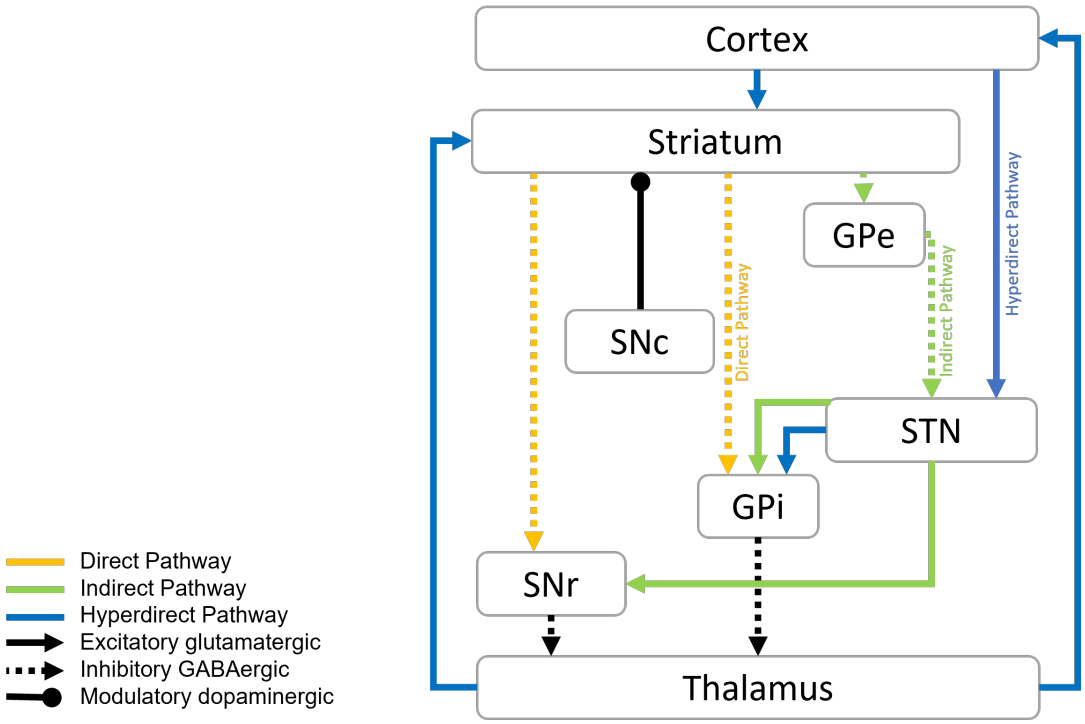

Figure 1.1: Overview of basal ganglia pathways.
The motor circuit consists of corticostriatal projections from the primary motor cortex and premotor cortex. There is an hyperdirect pathway that has direct glutamatergic connectivity from the motor cortex to the subthalamic nucleus (STN). The two main output nuclei of the basal ganglia are the globus pallidus internal (GPi) and substantia nigra *pars* reticulata (SNr), that project to the brainstem and ventrolateral thalamus. The striatal projections to these output nuclei are divided into direct and indirect pathways: the direct pathway is a monosynaptic connection between SPNs that express dopamine D1 receptors and GABAergic neurons in the GPi and the SNr; the indirect pathway originates from SPNs that express D2 receptors, which project to the globus pallidus external (GPe), and reach the GPi via the STN as a glutamatergic relay. Through these two pathways, the striatal dopaminergic tone regulates the GABAergic output activity of the basal ganglia [1]. SNc - substantia nigra *pars* compacta.

The direct pathway projects to the output nuclei in the basal ganglia which are the internal part of the globus pallidus and the substantia nigra *pars* reticulata. These consist of GABAergic neurons that maintain tonic activity and continuously inhibit their target cells in the ventral anterior and ventral lateral nuclei of the thalamus. These thalamic nuclei send glutamatergic projections to the frontal cortex, forming

the cortico-basal ganglia-thalamo-cortical loop. This pathway also has a net excitatory effect on the thalamus and cortex, which helps with the execution of motor activities [13].

The indirect pathway disinhibits the GABAergic neurons in the output nuclei in the basal ganglia, leading to reduced activity of the thalamic and cortical neurons, and suppression of undesired movements [13].

Some authors suggest that there is also an hyperdirect pathway in addition to the previous two. With a net inhibitory action on the thalamus and cortex, like the indirect projection, it bypasses the striatum and connects the frontal cortex to the output nuclei via glutamatergic neurons of the subthalamic nucleus [13].

Pre-synaptic terminals of excitatory synapses mostly release glutamate (Glu) as their major neurotransmitter. Glutamatergic synapses are almost exclusively located on dendritic spines. On the other hand, pre-synaptic terminals at inhibitory synapses primarily release GABA and unlike the previous, these synapses can be spread along the dendritic shaft, somata and axon initial segments [17].

Excitatory neurons can increase or decrease the accumulation of glutamate receptors at synaptic sites as a response to changes in their own firing rates. Therefore, in order to stabilize neuronal firing, they adjust its own synaptic strength to compensate for perturbations in surrounding neural activity [17]. Glutamate is possibly involved in neurodegenerative processes, with an excessive activation of glutamate receptors becoming excitotoxic and so contributing to the process of cell death in neurodegenerative disorders, namely in HD and PD [18, 19].

The inhibitory GABAergic interneurons stimulate and control network synchrony and oscillatory brain rhythms modulating synaptic efficacy. Previous studies suggested that impairment in inhibitory transmission blended with potential defects in homeostatic synaptic scaling at excitatory synapses which may possibly compromise the excitatory/inhibitory (E/I) balance critical to ensure proper functioning and plasticity of neural circuits. In fact, the disruption of the E/I homeostasis has been associated with neurodegenerative diseases [17].

1.2 Magnetic Resonance Spectroscopy as a non-invasive method for an *in vivo* biopsy of the brain

Nuclear magnetic resonance (NMR) is the underlying phenomena of magnetic resonance imaging (MRI) technique used to provide anatomical and functional images of the human body in a non-invasive manner. Relying on the physical-chemical properties of the nuclei that constitute the molecules and their interaction with magnetic fields, NMR spectroscopy was first used as a chemistry method to analytically identify molecules and to determine their biophysical characteristics. When used *in vivo*, to avoid confusion with other techniques, and the negative connotation with the word "nuclear", it started to be commonly referred to as magnetic resonance spectroscopy (MRS) [20]. MRS is therefore a technique broadly used in research and clinical studies, in particular proton MRS (^{1}H-MRS) due to the proton nuclei high natural abundance in the human body and MR signal sensitivity [20].

1.2.1 Structural and proton spectroscopic MR – How does it work?

The hydrogen nucleus is constituted by a single proton. Protons are positively charged particles that spin around their axis. Therefore, in the tissue, protons act as tiny magnets randomly oriented, in such a way that their magnetic fields, rather than summing up, eventually cancel out. However, if these protons are placed under a strong magnetic field (main magnetic field, B_0), the majority will align in the direction of the magnetic field whereas others will align in the opposite direction. Many protons will find their magnetic fields cancelled out, but an excess of protons will be aligned along the main magnetic field producing a net magnetization that spins around the main magnetic field at a frequency (Larmor frequency), proportional to B_0 [21]. By sending a radiofrequency (RF) pulse, in the same precessing frequency of the protons, these will absorb the RF energy and the net magnetization flips away from B_0 (excitation). When the RF pulse is turned off, there's a period of relaxation during which the protons re-align to B_0 and RF signals are generated and collected by a coil [22].

Hence the net magnetization is the source of the MR signal. The net magnetization may be represented by a vector constituted by two components: one in the

longitudinal direction, parallel to B_0 (z axis) – the longitudinal magnetization; and other in the transverse plane, orthogonal to B_0 (x-y plane) – transverse relaxation. Right after a 90° RF pulse, the net magnetization flips towards the x-y plane, and the longitudinal magnetization becomes zero, from where it will grow back in the longitudinal direction after the pulse is turned off. This is called longitudinal or T1 relaxation [21]. During the RF pulse, the protons start to precess together in the x-y plane, but right after it ends, they begin to dephase. This process of dephasing is called the T2 relaxation [21]. Both processes, T1 and T2 relaxation, happen at the same time. A few seconds after the RF pulse, most of the transverse magnetization is dephased and most of the longitudinal magnetization has grown back [21]. The rate at which longitudinal magnetization grows back and transverse magnetization decays after a RF pulse is different for different tissues due to its differences in water content having implications in the tissues contrast for either T1-weighted images or T2-weighted image [21]. To encode spatially the MRI signal, magnetic field gradients are used to produce small linear variations in B_0 intensity along space. Thus, with an MRI exam we will obtain an image with different contrast for different tissues. However, the MRS technique provides us with a spectrum. While the MRI signal is based on a single peak, the water peak, and its distribution and interaction with tissue, with MRS it is possible to distinguish a set of peaks at different RF representing proton nuclei in different chemical environments. Since the water signal is very strong when comparing to lower concentration proton-constituted metabolites, water suppression techniques are applied in order to detect the smaller metabolites [23], as described below.

Since it is a spectroscopy technique, ^{1}H-MRS detects RF signals that arise from hydrogen nuclear spins within tissue metabolites, which have chemical specific frequencies and that will be plotted in an MR spectrum. In this spectrum we have a plot of signal intensity versus the chemical shift of the metabolites [24]. The chemical shift is measured in a dimensionless unit, parts per million (ppm), by reference to a specific material [22] and corresponds to a nuclear behavior that depends on the chemical environment [22, 25]. Ppm are therefore a relative frequency (that varies with B_0) and since the ratio of the frequency is so modest, it shows in ppm. The electrons surrounding the nuclei create a magnetic field by interacting with B_0 [25], with protons in different sites experiencing different effective applied fields, and this has implications on the resonance frequency position of each peak [22,25]. This property can be used to distinguish different proton environments within molecules [22]. Depending on the shielding, which degree depends on the exact electronic environment, the NMR frequency can be shifted to lower or higher chemical shifts. In ^{1}H-MRS,

the chemical shift is often measured in reference to water at 4.7 ppm [22]. Summarizing, the MR spectrum is a combination of separable spectral patterns since metabolites resonate at different and specific frequencies.

Since in the MRS the water signal is suppressed, the region in which the MRS data is acquired must be first selected. Spectroscopy data is acquired from a well-defined voxel and there are two main types of localization methods that are commonly used. Single Voxel Spectroscopy (SVS) defines a small voxel of interest, which size is predefined by the user, within an organ, using three RF pulses with gradients defining three orthogonal planes that intersect to form the acquisition voxel, applied before the signal readout [22]. Smaller voxels contain smaller amounts of tissue producing a lower signal-to-noise ratio SNR [25]. To improve it, a higher number of signal averages are acquired, but leading to longer scan durations [22]. This means that choosing the right voxel size can be a matter of balance. Another way to conduct MRS experiments is through a hybrid MRS and imaging experiment, the Magnetic Resonance Spectroscopic Imaging (MRSI) also known as Chemical Shift Imaging (CSI) [24], which despite taking longer imaging times than SVS, and having lower SNR and higher contamination from adjacent voxels, it allows for the acquisition of smaller volumes in a wider coverage area than SVS.

Depending on the parameters used to obtain the spectrum, there are two predominant SVS techniques that can be used in ^{1}H-MRS *in vivo*: the STimulated Echo Acquisition Mode (STEAM) and the Point REsolved SpectroScopy (PRESS) [20]. STEAM permits shorter echo times, which improves resolution of the metabolites, but it is more sensitive to motion of the patients [25]. PRESS, on the other hand, is less sensitive to motion [25] and the signal intensity acquired is higher [22]. These two differ mostly in how the signal is produced; whereas STEAM uses magnetization to form a stimulated echo, PRESS measures spin echo [22].

1.2.2 Magnetic Resonance Spectroscopy - Clinical applications

MRS relies on the magnetic properties of certain nuclei and its surrounding chemical environment [20]. With this technique it is possible to detect relatively small molecules, in concentrations of 0.5 to 10 mM, either within cells or in extra-cellular spaces. MRS provides a MR spectrum, as a sum of sine waves of several peaks on unique resonance frequencies, with varied amplitudes, phases and relaxation properties, and shapes (due to spin couplings). Several metabolites may be then quantified

and information on metabolic pathways and neurotransmission tonus therein can indirectly be inferred, therefore making it suitable to monitor metabolic changes due to disease and to follow treatment [20].

The majority of the clinical MRS measurements are performed under field strengths of 1.5T or higher [20]. Our project will take advantage of a field strength of 3T. In comparison with lower field strengths, the SNR of MR spectra is improved, allowing to use smaller voxels [20].

MR spectra can be obtained from any nucleus possessing non-zero spin. Several metabolites can be quantified in the human tissue by targeting different nuclei, all of which can provide valuable metabolic or physiological information [20]. However, due to the high sensitivity of the protons, the wide availability of hydrogen and its abundant presence in most metabolites, ^{1}H-MRS is the most used in biomedicine [20,25]. Moreover, proton spectroscopy can be performed easily since it can be used with the help of a MR imaging system with standard RF coils developed for the acquisition of diagnostic MR images [20].

In the literature, the most suitable nuclei that have been used to obtain an MR spectrum are ^{31}P, ^{19}F, ^{13}C and ^{23}Na [2, 15]. ^{31}P-MRS can be used to investigate disturbed high-energy phosphate metabolism [20] and ^{13}C-MRS has been applied to uncover previously unknown disorders of N-acetylaspartate (NAA) synthesis, Glu neurotransmission, Krebs cycle, and glycolysis [20], for example.

There are several regular compounds/metabolites that can be identified in the spectra obtained from the human brain with a proton magnetic resonance obtained at field strengths inferior or equal to 3T. Some of these compounds include: myo-inositol (Ins), scyllo-inositol, glycerophosphocholine (GPC), phosphocholine (PC) and choline (Cho), creatine (Cr) and phosphocreatine (PCr), N-acetylaspartate (NAA), N-acetylaspartylglutamate (NAAG), glutamate (Glu), glutamine (Gln), γ-aminobutyrate, glucose, glutathione and lactate (Lac) [22, 26]. Glu and Gln combined are often referred to as Glx.

The most prominent signals in a ^{1}H-MRS spectrum are NAA, Cr e Cho [20, 24]. The NAA peak appears in the spectrum at 2.00 ppm and is usually the largest peak [25]. Its significance in the brain is quite complex, yet it has been associated with neuronal density and functional activity [27]. At 3.03 ppm, we can locate the peak of Cr, that has an additional peak visible at 3.94 ppm. This compound is especially involved in energy metabolism [20] and its concentration (associated with its peak amplitude in the MR spectrum) has been considered to remain quite

constant, even in presence of diseases, thus has often been used as a control/reference value for normalization purposes [25]. The Cho peak resonates at 3.2 ppm. It is one of the constituents of the phospholipid metabolism of cell membranes, reflecting membrane turnover. It is a precursor for phosphatidylcholine, used to build cell membranes, and for acetylcholine, a neurotransmitter involved in cognition, memory, and mood [25]. ^{1}H-MRS can also be used to quantify the levels of GABA and Glx (pool of glutamate and glutamine), which may provide an indirect evaluation of the E/I tonus in the brain [17]. However, while Glutamate is present in brain at relatively high concentrations, GABA is at the ^{1}H-MRS detection threshold level. After all, in the brain, five sixths of the neurons are glutamatergic and only a sixth are GABAergic [24]. Additionally, the dispersion of different signals along the chemical shift axis is limited when compared with the linewidth of signals masking the splitting of the signals associated with scalar J-coupling [28], which corresponds to a bond interaction responsible for the complex splitting of resonance lines in the spectra of molecules. Moreover, signals from different metabolites might overlap with less abundant metabolites such as GABA [24]. At 3T, the multiplets that arise from GABA protons overlap at 3.00 ppm with Cr signals, at 2.3 ppm with Glx and at 1.9 ppm with NAA signals [28]. New sequences for ^{1}H-MRS acquisition and new spectral editing techniques have been proposed [29, 30].

The levels of each metabolite can be estimated as the area under each assigned peak. However, these are relative concentrations, and the absolute concentration of the metabolite remains unknown. One solution is to use an external reference standard containing metabolites at an *a priori* known concentration. Instead, it is common to make all measures relative to an internal reference, which concentration may itself be based on assumptions and peak estimations such as tissue water (assessed through a short ^{1}H-MRS acquisition without water suppression) or other metabolites that are considered to be constant [31].

On this premise, the concentration values are normally described in ratios. As mentioned earlier, a common denominator for brain spectra is Cr. The values obtained should be compared with a reference dataset obtained in healthy volunteers using identical procedures in the same institution, since these concentration values change with the location of the Volume of Interest (VOI), the voxel tissue composition, as well as with patient age [20]. The most notable variation is an increase in NAA/Cr ratio and a decrease in the Cho/Cr ratio as the brain matures [25].

Two sequences in spectral editing have been frequently used, to analyze the low-concentration metabolites, essential to distinguish overlapping peaks: the MEscher-

GArwood Point Resolved SpectroScopy (MEGA-PRESS) and the Hadamard Encoding and Reconstruction of MEGA-Edited Spectroscopy (HERMES) sequences. The later allows the simultaneous acquisition of more than two edited signals from molecules, whereas MEGA-PRESS can only detect one molecule at a time [32]. In this project the MEGA-PRESS sequence was applied to estimate GABA and Glx levels, therefore more details on this sequence are described in the Methods section.

1.3 Objetive/Motivation

In this project, we aim to study the excitatory/inhibitory balance, *in vivo*, of the frontal cortex of Huntington's and Parkinson's Disease patients, as compared with healthy Control participants, by estimating the levels of the main excitatory (Glx, the pool of glutamate and glutamine, as an approximation for glutamate) and inhibitory (GABA, γ -aminobutyric acid) neurotransmitters, using proton Magnetic Resonance Spectroscopy (^{1}H-MRS), which is potentially relevant as a diagnostic and therapeutic prediction biomarker.

2

Methods

2.1 Cohort Description

Seventy subjects enrolled this Project (Table 2.1), one patient in the HD group was excluded prior to any analysis: 27 patients with **Parkinson's Disease** diagnosis (13 males, mean age ± SD = 55.0 ± 10.00 years, disease duration ± SD = 3.8 ± 2.29 years); 27 patients (one HD patient was excluded since proton spectroscopy data was acquired, not in the frontal lobe (more details in the sub-section *2.2.1. MRI and ^{1}H-MRS data acquisition*), but in the right basal ganglia, focusing the right putamen) diagnosed with **Huntington's Disease** (26 HD, 8 males; mean age ± SD = 42.3 ± 9.89 years, disease duration ± SD = 5.3 ± 3.10 years (n=14)); and 16 **Control** subjects (5 males, mean age ± SD = 40.5 ± 9.47 years). Within the PD group, 17 were early-stage idiopathic and 9 were early-onset Parkinson's Disease patients. One PD patient was a carrier of a mutation on the LRRK2 gene. In the HD group (26 participants), 14 patients could be classified as early manifest and 12 as premanifest Huntington's Disease patients. PD and HD subjects were recruited from the Movement Disorders Unit of the Neurology Department of Coimbra University Hospital Centre and most control participants were gene negative or non-at-risk relatives of the HD affected participants and clinical criteria defining each groups/sub-groups were described elsewhere [33, 34]. Exclusion criteria included: for clinical groups, dementia, severe depression, history of substance abuse, or any other neurological condition; for healthy control participants, history of dementia, depression or any neurologic or psychiatric disorder, substance abuse, or the use of psychotropic medication. PD and HD participants were assessed in their regular on-state of medication.

Informed written consent was obtained from each participant following the tenets of the Declaration of Helsinki after procedures of the research had been fully explained. The study was approved by the Ethics Committees of the Faculty of Medicine and

of the Coimbra University Hospital.

Table 2.1: Clinico-demographic characterization of the participants from the initial Parkinson's Disease (PD), Huntington's Disease (HD) and Control groups.

	PD	HD	Control
n	27	26	16
Sex (males)	13	8	5
Age (y)	55.0 ± 10.00	42.3 ± 9.89	40.5 ± 9.47
BMI (kg/m^2)	27.1 ± 4.06	22.7 ± 3.38 (n=20)	24.9 ± 3.58
Disease Duration (y)	3.8 ± 2.29	5.3 ± 3.10 (n=14)	NA

Quantitative data is represented as mean ± SD values and qualitative data as absolute frequencies.
BMI – Body Mass Index; NA – Not Applicable.

2.2 Data Analysis

2.2.1 MRI and ^{1}H-MRS data acquisition

Magnetic resonance imaging data (structural and proton spectroscopy) was acquired using a 3T MRI scanner (Siemens Magnetom TimTrio, Erlangen, Germany), with a 12-channel birdcage head coil, at the Institute of Nuclear Sciences Applied to Health, University of Coimbra.

For each participant, the MRI protocol started with the acquisition of a high-resolution anatomical T1-weighted MR image, based on the Magnetization Prepared Rapid Acquisition Gradient Echo (MPRAGE) with the following parameters: repetition time (TR) 2530 ms, echo time (TE) 3.42 ms, flip angle (FA) 7°, field of view (FoV) 256 x 256 mm^2, yielding 176 slices with 1 x 1 x 1 mm^3 voxel size. These images were used for spectroscopic voxel placement and segmentation of tissues within the voxel.

To estimate the levels of GABA and Glx, we used MEscher-GArwood Point Resolved SpectroScopy (MEGA-PRESS) sequence [62] with the following parameters: TR = 1500 ms, TE = 68 ms, 392 averages, 1024 data points. ^{1}H-MRS data was acquired in a 3 x 3 x 3 cm^3 voxel anatomically positioned medially in the frontal lobe (Figure 2.1).

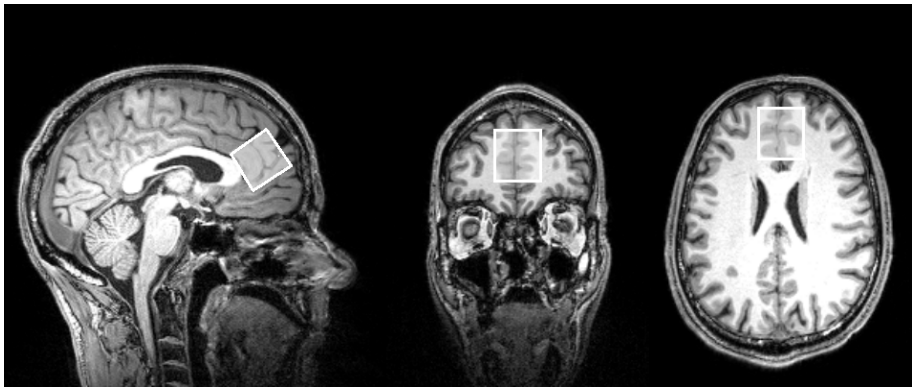

Figure 2.1: Representative image of ^{1}H-MRS voxel positioning in the medial frontal lobe of a PD patient (male, 47y) shown in the sagittal, coronal and axial orthogonal planes, from left to right.

The frontal lobe was chosen due to its tight connectivity with basal ganglia [35]. The voxel's size was a compromised solution, between the enclosed amount of tissue, improving the signal-to-noise ratio, and the localization, to be accommodated within the frontal lobe but preventing other structures contamination as bone and ventricles. For quantification of the water-scaled metabolites levels, MEGA-PRESS data with no water suppression (NWS) were also acquired in the same location (TR = 1500 ms, TE = 68 ms, 16 averages, 1024 data points). This acquisition also allows to correct for eddy-currents, improving the signal quality [36]. In MEGA-PRESS, during odd number acquisitions (196 averages), a frequency-selective inversion pulse was applied to the GABA-C3 resonance at 1.9 ppm (ON) and, during even number acquisitions (196 averages), the pulse was applied at 7.5 ppm (OFF). ON and OFF spectra were subtracted offline to retrieve GABA and Glx peaks (more details are presented in the next subchapter).

2.2.2 MEGA-PRESS: a J-difference editing method to estimate GABA in ^{1}H-MRS

MEGA-PRESS is a popular technique used to estimate more accurately GABA *in vivo* [31], due to its ability to edit low-concentration metabolites [37] that are often overlapped by stronger signals that resonate at similar frequencies by taking advantage of known couplings within the GABA molecule [31] and returning a GABA signal more robust than other techniques (for example, standard PRESS). The GABA molecule consists of six coupled proton spins which chemical shifts are

at 3.01 ppm, 2.28 ppm and 1.89 ppm [28]. This technique removes overlapping contributions of other metabolites such as Cr that, like GABA, appears at around 3.00 ppm. Nonetheless, one limitation is that the MEGA-PRESS targeting GABA still has contributions of other coedited signals such as macromolecules and homocarnosine. Thus, in the literature, very often it is referred to as GABA+ [38].

MEGA-PRESS is a J-difference editing technique that implies the acquisition of two sub-spectra, an ON and OFF spectra. During the ON spectra acquisition, an editing pulse is selectively applied to GABA spins at 1.90 ppm, to refocus the evolution of J-coupling to the 3.00 ppm GABA spins. During the OFF spectra acquisition, an inversion pulse is applied at a frequency with no impact on GABA signals (7.50 ppm), so that the J-coupling evolves freely throughout the echo time. These editing pulses do not affect most of peaks in the spectrum, hence by subtracting the OFF from the ON spectrum the majority of the peaks are removed, leaving a final spectrum with only those signals that were affected by the editing pulses, namely the 3.00 ppm GABA signal [31].

Therefore, the difference spectrum (Figure 2.2) shows signals close to 1.9 ppm that were directly targeted by the pulses; the 3.00 ppm GABA signal, coupled to 1.90 ppm GABA spins; the glutamate/glutamine pool (Glx) signal at around 3.75 ppm, coupled to the ∼2.10 ppm Glx resonances; and some J-coupled macromolecular peaks [31].

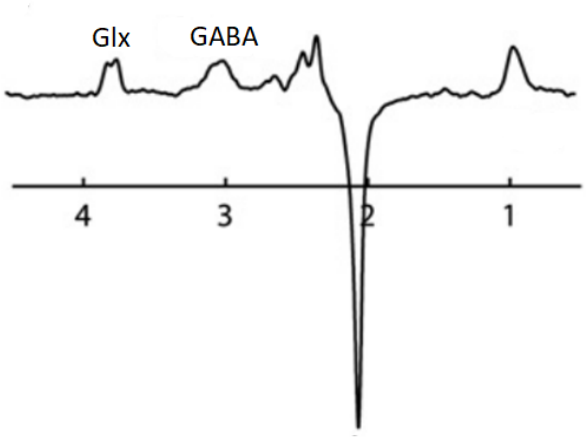

Figure 2.2: Representative MEGA-PRESS edited spectrum with GABA (∼3.00 ppm) and Glx (∼3.75 ppm) peaks highlighted on top (adapted from [29]).

Generally, metabolites levels are expressed as ratios relative to an internal reference metabolite assumed to be stable. There are three references that are often used: Cr, water and NAA [39]. Cr and NAA have the advantage that they are acquired simultaneously during the same MEGA-PRESS scan, minimizing potential effects of patients' movements, partial volume effects, hardware instabilities, etc, reducing inter-subject variability. Cr has an additional advantage as its main resonance is very close to the edited GABA signal, meaning the chemical shift displacement issues will be minor. However, the signal stability must be misleading and other approaches should be taken into consideration [40]. The water signal, on the other hand, has higher SNR and is more easily modeled since the proton MRS without water suppression reveals a well resolved peak that can be later used as an endogenous concentration reference [31].

2.3 Data Processing

To analyze MEGA-PRESS data and estimate GABA and Glx levels, we applied a spectral analysis pipeline using Gannet version 3.1 [41], an open-source toolbox for MATLAB (R2019a, TheMathWorks, USA).

Gannet makes several assumptions, for example, with the shape of the data, while processing it. Gannet uses non-linear least-squares fitting to integrate the $\sim$ 3.00 ppm of GABA and Cr and the 3.75 ppm Glx peaks. Each signal was modelled to different functions: for **GABA** signal, a Gaussian model was applied in the difference spectrum; the **Glx** signal was modeled from a three-Gaussian function; for the **Cr** signal, a Lorentzian model was applied in the OFF spectrum; and the **water** signal from the unsuppressed water spectrum, was modeled by a mixed Gaussian-Lorentzian function [41].

Gannet processing pipeline follows an orderly workflow of four steps that are executed with the Matlab commands: GannetLoad, GannetFit, GannetCoRegister and GannetSegment [41]. In the later versions, a new command was added to the toolbox, GannetQuantify. Before starting to analyze the data, some settings were specified in GannetPreInitialise (Appendix A), such as the order of ON and OFF acquisitions (in our study, ON acquisitions took place first).

The first step is ***Loading*** in which time-domain MRS raw data acquired with the MRI scanner are preprocessed. Signal processing in the time domain, minimizes the

impact of artefacts and unwanted noise within the data [22]. First, a frequency and phase correction was applied to the time-domain raw data and then a 3 Hz exponential apodization function or line broadening before converting data to frequency domain through the Fast Fourier Transform (FFT). Before subtracting ON and OFF spectra, a frequency and phase correction was applied on frequency domain data by using the parameters from the modeling of the creatine and choline signals in the OFF spectra to diminish subtraction artifacts [41]. Unsuppressed water data were also processed similarly. Finally, ON and OFF spectra are subtracted to obtain the edited difference spectrum to be analyzed. Since the data were collected and retrieved as Siemens RDA files, these spectra are already time-averaged limiting the extent of preprocessing approaches.

The second step is the ***Fitting***, in which fitting models are applied to the metabolites of interest in the preprocessed data. A nonlinear least-squares fitting is used to integrate the edited GABA and Glx peaks at around 3.00 ppm and 3.75 ppm producing GABA and Glx levels estimations [41]. It does the same for Cr and unsuppressed water data, when provided, which was the case. Results are then presented as:

I) The integrals ratio (C) of GABA (or Glx) and Cr (Equation 2.1),

$$C = \frac{I_M}{I_{Cr}} \tag{2.1}$$

where I_M is the metabolite (GABA or Glx) signal integral and I_{Cr} is the creatine signal integral [42], or;

II) An absolute concentration (C_M), in "institutional units" (i.u.), relative to water (Equation 2.2) [41],

$$C_M = \frac{I_M}{I_W}\frac{H_W}{H_M}\frac{MM}{\kappa}C_W W_{vis}\left\{\frac{\exp\left(-\frac{TE_W}{T_{2W}}\right)\left[1-\exp\left(-\frac{TR_W}{T_{1W}}\right)\right]}{\exp\left(-\frac{TE_M}{T_{2M}}\right)\left[1-\exp\left(-\frac{TR_M}{T_{1M}}\right)\right]}\right\} \tag{2.2}$$

where κ is the editing efficiency of the sequence (currently set to 0.5 for GABA and 0.4 for Glx, TE=68 ms); C_W the molal concentration of pure water (55 mol/L); TE and TR, the echo and repetition time respectively of the experiment for

metabolite (TE_M, TR_M) and water reference acquisitions (TE_W, TR_W); T_{2W} and T_{2M}, the transverse relaxation times of water (0.095 s, average of T2 of water in WM and GM) and the metabolites (GABA, 0.088 s; Glx, 0.18 s), respectively; T_{1W} and T_{1M}, longitudinal relaxation times of water (1.100 s, average of T1 of water in WM and GM) and the metabolites (GABA, 1.31 s; Glx, 0.18 s), respectively; H_W and H_M, the number of ^{1}H that originate the water (2) and the metabolites (GABA, 2, Glx, 1) signals, respectively; W_{vis}, the average relative visibility of water in GM and WM (0.65); MM, the correction factor to account for the contribution of the co-edited macromolecules signals in the GABA (0.45) and Glx (1) signals; and I_M and I_W, the integrals of the modeled peaks fitting the GABA (or Glx) and water spectra, respectively [41,42]. These parameters were used by default (set in Gannet script), based on the reported literature.

Besides the peaks' integrals estimation, Gannet also calculates normalized residuals for each fit (for GABA, R_{GABA}), as the standard deviation (SD) of the fitting residual divided by the amplitude of the fitted peak. The normalized residuals for GABA (and Glx) and Cr may be combined ($E_{M,Cr}$) to obtain an estimate of the overall fit error (Equation 2.3) [41]:

$$E_{M,Cr} = \sqrt{R_M^2 + R_{Cr}^2} \tag{2.3}$$

We will analyze these fit errors, that reflect the quality of the fitting provided by Gannet, as well as the full-width-at-half-maximum (FWHM) linewidths of the modeled peaks (Hz) and the SNR values, to indirectly access the quality of the spectra.

The output reported by GannetLoad and GannetFit from one HD patient are shown in Figure 2.3.

The third step is the ***CoRegistering***, in which the MRS voxel is co-registered to the participant' brain anatomical image to prepare for the fourth step, the ***Segmentation***. During segmentation, the MRI structural image is segmented into the three major tissues found in the brain (gray matter (GM), white matter (WM) and cerebrospinal fluid (CSF)) [43]. Then, by overlaying the voxel as a mask it is possible to estimate each tissue fraction enclosed within it. These two steps require the algorithms of another Matlab toolbox, the SPM12 toolbox (The Wellcome Trust Centre for Human Neuroimaging, Institute of Neurology, UCL, London, UK, https://www.fil.ion.ucl.ac.uk/spm/). These tissue fractions were used to correct for

distinct metabolites distributions in different compartments (more details below).

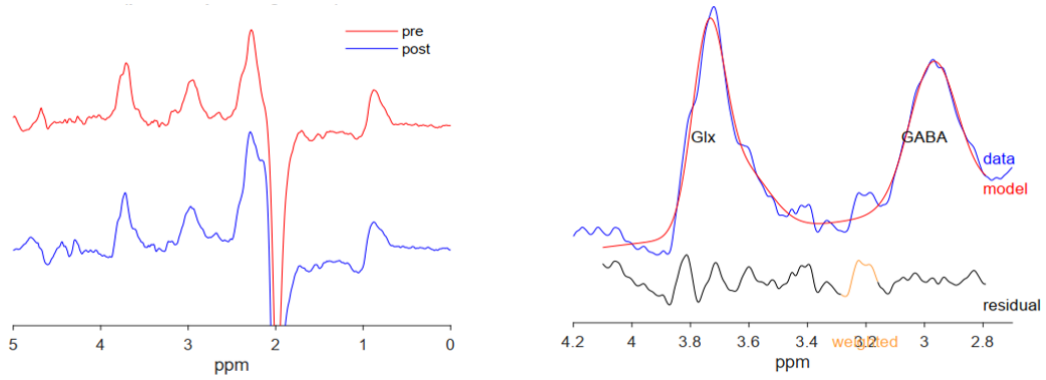

(a) GannetLoad output **(b)** GannetFit output

Figure 2.3: Representative edited spectra of a HD patient. During (a) GannetLoad, data was preprocessed and aligned (bottom blue line) and after, during (b) GannetFit, the edited post-processed spectrum (blue) was fit by a model (red) to estimate GABA and Glx peak integrals. In (b) residual data is shown at the bottom in black.

Gannet version 3.1 has a fifth module, GannetQuantify. In this module the ***Quantification*** of the metabolites' levels is corrected for partial tissue volume effects [44], using the obtained data from tissue segmentation. The method we followed to analyze corrected metabolite measurements was the tissue correction with an alpha factor (Equation 2.4) [42, 45]. Accordingly, this algorithm will return a metabolite concentration (C_{corr}, in i.u.) that considers tissue fractions within the voxel as well as an alpha ponderation accounting for the regional differences of metabolites concentration in GM, WM and CSF.

$$C_{corr} = \frac{I_M}{I_W}\frac{H_W}{H_M}\frac{MM}{\kappa}\left\{\frac{\sum_i^{GM,WM,CSF} f_i C_{W,i}\exp\left(-\frac{TE_W}{T_{2W,i}}\right)\left[1-\exp\left(-\frac{TR_W}{T_{1W,i}}\right)\right]}{\exp\left(-\frac{TE_M}{T_{2M}}\right)\left[1-\exp\left(-\frac{TR_M}{T_{1M}}\right)\right]}\right\}\frac{1}{f_{GM}+\alpha f_{WM}} \quad (2.4)$$

Some parameters, κ, I_M, I_W, H_W, H_M, MM, TE_W, TE_M, TR_W, TR_M are the same as in Equation 2.2. New parameters include: f_i, the volume fraction of GM (f_{GM}), WM (f_{WM}) or CSF within the MRS voxel; $C_{w,i}$, the molal concentration of pure water in each tissue (GM, 43.30 mol/kg, WM, 36.08 mol/kg, CSF, 53.84 mol/kg, considering the molal concentration of pure water, 55.51 mol/kg); T_{1M} and T_{2M}, the longitudinal (GABA, 0.088 s; Glx, 0.18 s) and transverse (GABA, 1.31 s;

Glx, 0.18 s) relaxation times of the metabolites; $T_{1W,i}$ and $T_{2W,i}$, the longitudinal and transverse relaxation times of water in GM ($T_{1,GM}$, 1.331 s; $T_{2,GM}$, 0.110 s), WM ($T_{1,WM}$, 0.832 s; $T_{2,WM}$, 0.0792 s) and CSF ($T_{1,CSF}$, 3.817 s; $T_{2,CSF}$, 0.503 s); and α (0.5), that accounts for different concentrations of the metabolites in GM and WM, considering a ratio of 1:2 (WM/GM) [42, 45].

Gannet is a useful tool because it requires barely any user-input [41] making it less promptly to human error. After defining the parameters to be used in the GannetPreInitialise batch (Appendices A), sometimes, depending on patients data, some adjustments were required: the order of the editing pulses (MRS_struct.p.ONOFForder) needed to be changed from "onfirst" to "offfirst"; and the MRS_struct.p.AlignTo would need to be adjusted from "RobustSpecReg", a more robust correction of frequency and phase errors [46], to "SpecReg", in order to have the best processed data for modelling and quantification. In our study, out of the 69 initial datasets, for 28 (PD, $n = 12$; HD, $n = 11$; Controls, $n = 5$) "offfirst" was used and for 11 (PD, $n = 5$; HD, $n = 3$; Controls, $n = 3$) "SpecReg" was used. Only 1 PD patient spectrum improved with both mentioned adjustments. This patient's data was used for further analysis. Despite trying to improve the spectra with these adjustments, in most cases the improvements were still insufficient to pass the visual quality control screening performed during Gannet analysis based on previous knowledge about the expected spectral behavior. Among the qualitative visual exclusion criteria were identified: very noisy spectra; misplaced peaks in the ppm scale (shifted to values either higher or lower than the expected); and inaccurate model fittings (representative examples in Figure 2.4).

Other exclusion criteria, more objective than visual inspection, should be also used after model fitting. Those include analysis of SNR, FWHM and CRMVB (Cramer-Rao minimum variance bounds), a criterion more linked to confidence limit, that reflects stochastic uncertainty for single measurements and depends on SNR and the inherent limits of the fitting model. Merely stating SNR or FWHM is considered an inferior way to judge the quality of quantified data when compared with analyzing CRMVB. However, systematic errors are neglected and may lead to over- or underestimated confidence limits [47]. In Gannet, CRMVB are not estimated. However, we used not only FWHM and SNR, but also Fit Errors (Equation 2.3), as approximate measures to evaluate model fitting quality.

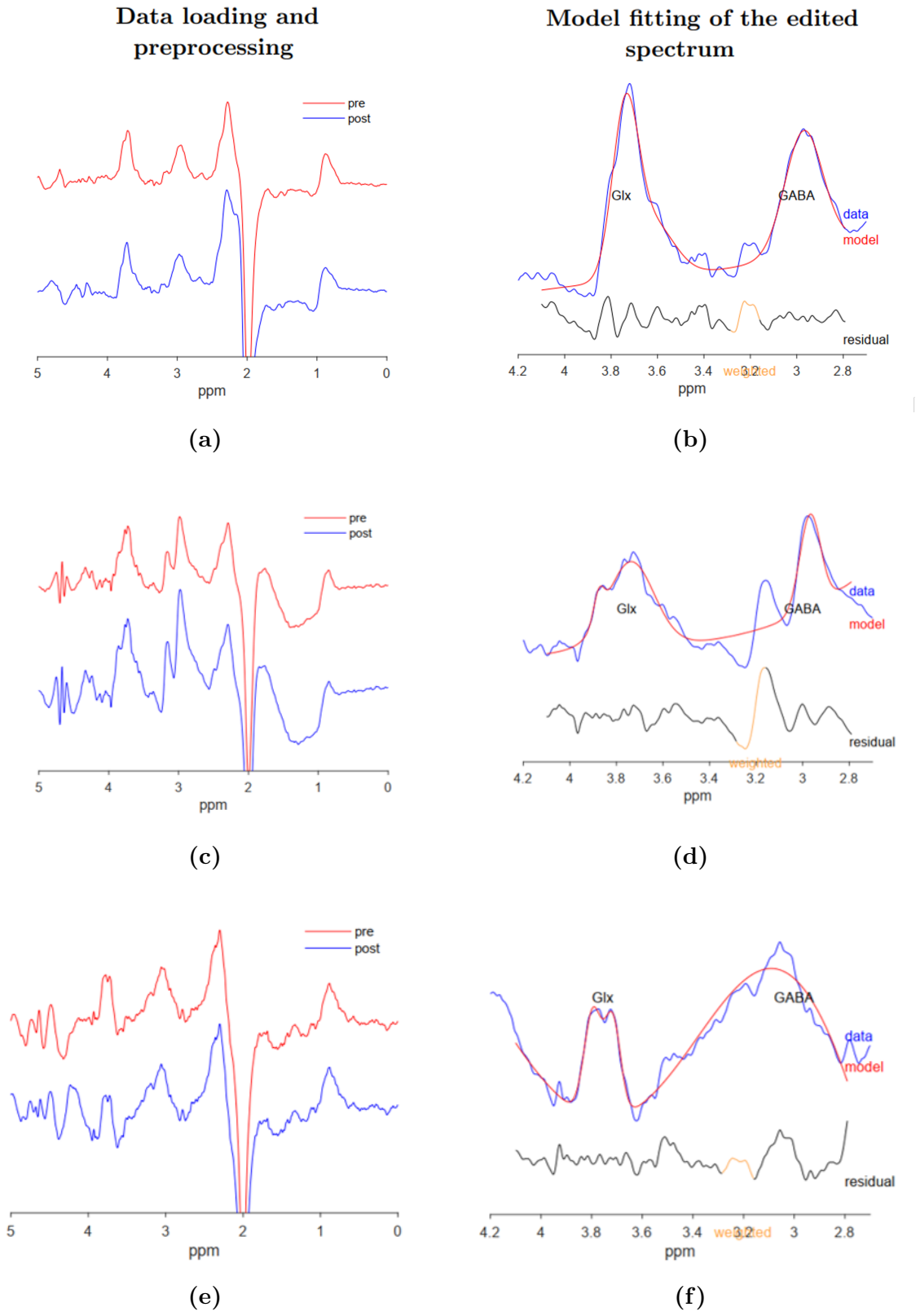

Figure 2.4: Examples of spectra after Gannet pre-processing (left) and fitting (right) steps of three representative HD patients. After visual quality control analysis, on top (a,b), data was further included; however, in (c-f) data were excluded due to high noise contamination and weak signal modeling (due to bad signal shapes).

In this study, metabolite levels results were analyzed as the ratios of GABA and Glx relative to Cr (Equation 2.1) and relative to water, in institutional units (i.u.), corrected for tissue fraction (Equation 2.4). We will herein keep the term GABA along the text but bearing in mind that this signal has contributions of homocarnosine and macromolecule signals.

2.4 Statistical analysis

Statistical analysis was performed using R Statistical Software, version 4.1.0 [48]. Proportion analysis of qualitative variables such as sex within groups, were performed with a Chi-Squared Test. The Shapiro-Wilk test was applied to the quantitative clinical-demographic variables (age, BMI and disease duration) for data normality evaluation. If normality assumption was verified, group comparisons were performed with one-way ANOVA, otherwise equivalent nonparametric Kruskal-Wallis Test were used instead. When adequate, *post-hoc* tests with multiple comparisons correction were applied: Tukey after ANOVA and Benjamini-Hochberg (BH) correction after Kruskal-Wallis tests. To compare disease duration between HD and PD groups, a Mann-Whitney-Wilcoxon (rank sum) test was applied after data normality was not verified.

Following the initial visual quality control screening, 44 participants (PD, $n = 21$; HD, $n = 13$; Controls, $n = 10$) were removed from further analysis. Considering the low sample sizes, we opted to proceed with non-parametric tests. Thus, analysis on the final cohorts' clinical-demographic characteristics was repeated and between groups (PD, HD and Control groups) comparisons of tissue fractions (GM, WM and CSF) within the voxel, GABA and Glx levels (ratios to both Cr and to water) and quality measures (Fit Error, FWHM and SNR) were performed through the Kruskal-Wallis Test. If significant differences were found, pairwise comparisons with BH adjustment were applied. All tests were performed two-tailed with a 5% significance level.

Due to the drastic decrease of our sample size ($n = 25$), a *post-hoc* analysis was additionally performed. G*Power, version 3.1 [49], was used to estimate the achieved power of the main analysis and to calculate the adequate sample size required to obtain a statistically significant effect size. Two different approaches were considered, as follows:

I) Power Estimation. Given our sample sizes and the mean ± SD values of the Glx/GABA ratio (based on the absolute values of the metabolites corrected for tissue fraction) to calculate the effect size, we estimated the power achieved in our analysis considering pairwise comparisons between PD vs. Controls, and HD vs. Controls with a two-tailed Wilcoxon-Mann-Whitney test, and an alpha of 0.05.

II) Sample size calculation. The estimated effect size was calculated with the mean ± SD values of the Glx/GABA ratio (based on the absolute values of the metabolites corrected for tissue fraction) obtained in this project, as preliminary data. The sample sizes estimations (allocation ratio = 1) were performed for pairwise differences between PD vs. Controls, and HD vs. Controls, with an independent samples t-test with the following input parameters: two-tailed test, alpha of 0.05, and power of 0.80.

3

Results

3.1 Demographic data

As previously described, MEGA-PRESS ^{1}H-MRS data were acquired in a cohort of 70 participants (Table 3.1). This cohort was divided in two clinical groups (Parkinson's Disease and Huntington's Disease) with 27 subjects each and one control group ($n = 16$). In all participants, proton spectroscopy data was acquired in a frontal 27cm^3 voxel, except for one HD patient. Thus, this patient was excluded (details in *Methods* section).

The proportion of males (and females) was identical in all groups (Pearson $\chi^2(2) = 2.07$; $p = 0.355$). One-way ANOVA results showed a significant difference of mean age ($F(2,66) = 15.49$, $p < 0.001$) and BMI ($F(2,60) = 7.96$, $p < 0.001$) between groups, as partially expected from differences in age of disease onset. Statistically significant differences (*post-hoc* tests with Tukey correction) on age means were verified between PD group (higher mean) and both HD ($p < 0.001$) and Control ($p < 0.001$) groups, but not between HD and Control groups. For BMI, differences were only found between HD and PD groups ($p = 0.001$), the former with lower BMI mean. Disease duration was not significantly different between the two clinical groups (Mann-Whitney-Wilcoxon (rank sum) test, $n_{HD} = 14$, $n_{PD} = 27$, W = 242, $p = 0.144$).

However, after a visual quality control assessment, prior to model fitting and metabolites' level estimation, 44 datasets were fully discarded. Descriptive analysis of the remaining participants' clinical-demographic data is reported in Table 3.1 (bottom).

Table 3.1: Brief clinical-demographic description of Parkinson's Disease (PD), Huntington's Disease (HD) and Control cohorts included in the initial sample and those included after visual quality control inspection of preprocessed edited spectra.

	PD	HD	Control	Statistic (p-value)
n	27	26	16	
Sex (males)	13	8	5	0.355
Age (y)	55.0 ± 10.00	42.3 ± 9.89	40.5 ± 9.47	< 0.001
BMI (kg/m^2)	27.1 ± 4.06	22.7 ± 3.38 (n=20)	24.9 ± 3.58	0.001
Disease Duration (y)	3.8 ± 2.29	5.3 ± 3.10 (n=14)	NA	0.144
Clinical-demographic characterization of the final cohorts after visual quality control assessment				
n	6	13	6	
Sex (males)	2	5	1	0.851
Age (y)	53.0 ± 9.49	43.1 ± 6.70	42.0 ± 10.10	0.099
BMI (kg/m^2)	24.4 ± 3.11	23.0 ± 2.84 (n=9)	24.8 ± 3.92	0.492
Disease Duration (y)	3.8 ± 3.76	7.0 ± 2.83 (n=6)	NA	0.106

Quantitative data is represented as mean ± SD values and qualitative data as absolute frequencies.
BMI – Body Mass Index; NA – Not Applicable.

In this new scenario, the proportion of males (and females) was identical in all groups (Fisher-Freeman-Halton Exact Test, $p = 0.851$). Kruskal-Wallis results showed no significant differences on age ($H(2) = 4.63$, $p = 0.099$) or BMI ($H(2) = 1.42$, $p = 0.492$) between groups. Disease duration was not significantly different between the two clinical groups (Mann-Whitney-Wilcoxon (rank sum) test, n_{HD}=6, n_{PD}=6, W = 28.5, $p = 0.106$).

3.2 GABA and Glx Concentrations

In this work, metabolite levels were expressed as ratios of GABA and Glx relative to water (GABA/W, Glx/W), in institutional units (i.u.), and relative to Cr (GABA/Cr, Glx/Cr).

Studies show that GABA and also Glutamate are distinctively distributed in gray matter (GM), white matter (WM) and cerebrospinal fluid (CSF) [45, 50]. Metabolites are specially elevated in GM, lower in WM and being almost residual in CSF. In addition, relaxation times for the metabolites in the different tissues must be

accounted. Therefore, anatomical images were segmented, and the percentages of each tissue type enclosed in the spectroscopy voxel were estimated (Table 3.2).

Table 3.2: Mean tissue fraction (mean ± SD) for Parkinson's Disease (PD), Huntington's Disease (HD) and control participants.

	PD	HD	Control	p-value
n	6	13	6	
GM (%)	49.02 ± 3.21	50.66 ± 2.51	51.25 ± 2.20	0.314
WM (%)	30.45 ± 4.27	29.80 ± 3.83	33.43 ± 2.35	0.116
CSF (%)	20.53 ± 4.37	19.55 ± 4.07	15.37 ± 1.94	0.008

Analyzing voxels composition, Kruskal-Wallis results showed no significant differences on GM ($H(2) = 2.32$, $p = 0.314$) or WM ($H(2) = 4.31$, $p = 0.116$) fractions between groups. However, significant statistical differences were found for CSF fraction ($H(2) = 9.62$, $p = 0.008$. *Post-hoc* pairwise tests with BH adjustment showed statistically significant differences of CSF fraction between the Control group (lowest median CSF fraction) and both PD ($p = 0.007$) and HD ($p = 0.016$) groups, but not between HD and PD groups.

In order to control for the GM, WM and CSF content and tissue relaxation properties, metabolites levels were also estimated (GABA/$W_{(\alpha c)}$, Glx/$W_{(\alpha c)}$) using the equation previously described in the Methods section (Equation 2.4). These were considered more robust measures of metabolites concentration, ergo these were our main variables of interest.

Median (IQR) of GABA and Glx levels for each group, are presented in Table 3.3, and the distributions of the individual values are represented in Figure 3.1.

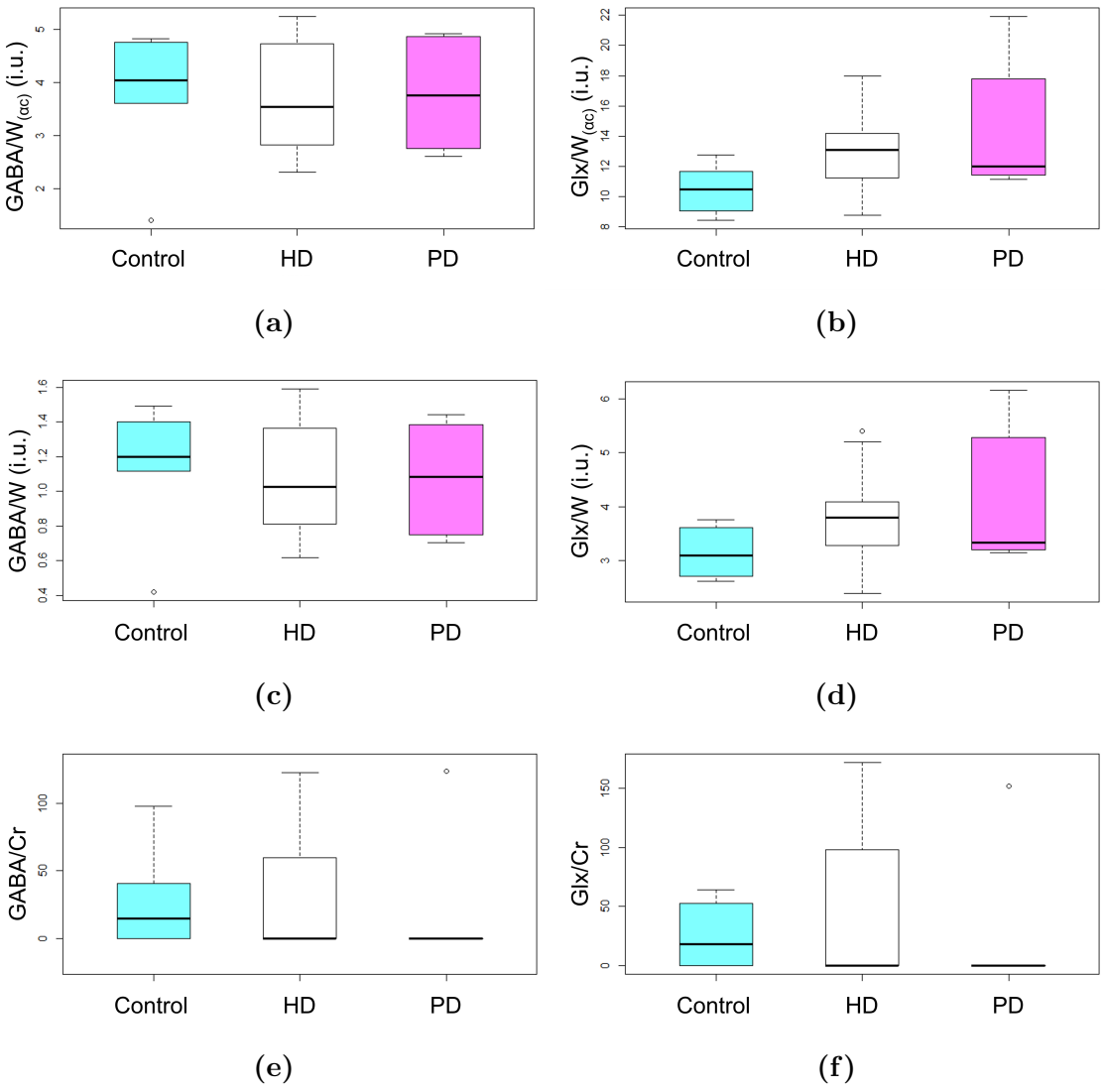

Figure 3.1: Distribution of GABA (right) and Glx (left) levels (a,b) relative to water with α tissue correction ($GABA/W_{(\alpha c)}$, $Glx/W_{(\alpha c)}$), in institutional units (i.u.); (c,d) relative to water, without tissue correction, (GABA/W, Glx/W), in institutional units (i.u.); and (e,f) relative to Cr (GABA/Cr, Glx/Cr), in Parkinson's Disease (PD), Huntington's Disease (HD) and healthy Control group.

Table 3.3: Neurotransmitter levels (median (IQR)) relative to water with α tissue correction (GABA/$W_{(\alpha c)}$, Glx/$W_{(\alpha c)}$), relative to water, without tissue correction, (GABA/W, Glx/W), and relative to Cr (GABA/Cr, Glx/Cr) in the frontal lobe of Parkinson's Disease (PD), Huntington's Disease (HD) and Control participants. i.u. - institutional units

	PD	HD	Control	Statistic (p-value)
n	6	13	6	
GABA/$W_{(\alpha c)}$ (i.u.)	3.75 (1.71)	3.54 (1.91)	4.04 (0.88)	0.922
GABA/W (i.u.)	1.08 (0.52)	1.03 (0.55)	1.20 (0.23)	0.846
GABA/Cr	0.13 (0.06)	0.19 (59.34)	14.71 (37.84)	0.228
Glx/$W_{(\alpha c)}$ (i.u.)	11.99 (4.92)	13.10 (2.93)	10.47 (2.35)	0.339
Glx/W (i.u.)	3.33 (1.56)	3.80 (0.81)	3.10 (0.77)	0.253
Glx/Cr	0.12 (0.10)	0.18 (97.71)	18.32 (48.37)	0.543

Statistical analysis showed no significant differences between groups in the levels of GABA (GABA/$W_{(\alpha c)}$: $H(2) = 0.16$, $p = 0.922$; GABA/W: $H(2) = 0.33$, $p = 0.846$; GABA/Cr: $H(2) = 2.96$, $p = 0.228$) or Glx (Glx/$W_{(\alpha c)}$: $H(2) = 2.16$, $p = 0.339$; Glx/W: $H(2) = 2.75$, $p = 0.253$; Glx/Cr: $H(2) = 1.22$, $p = 0.543$), regardless the estimation approach. After inspecting the descriptive data (Table 3.3 and Figure 3.1), ratios to Cr were far from the expected. Close analysis showed that, in these cases, the peak of creatine was inverted and/or not well defined, then the modelling and estimation failed (representative "good" and "bad" Creatine fittings is reproduced in Figure 3.2, and more details on the spectra quality are reported in the next Results sub-section, *3.3. Spectral quality assessment*).

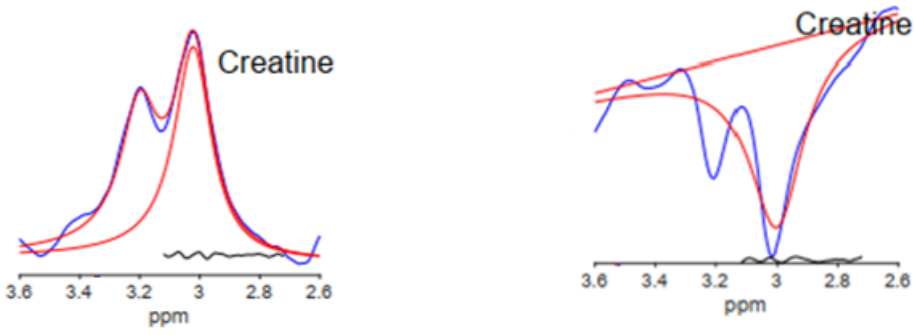

(a) **(b)**

Figure 3.2: Representative Gannet fitting to model Creatine peak at 3.00 ppm. In (a) there was a good model fitting (HD, female, 25y) and in (b) the model fitting failed since the creatine peak is inverted (PD, male, 56y).

Despite the absence of differences on individual levels of GABA and Glx, E/I balance was indirectly assessed by comparing Glx and GABA ratio between the three groups (Table 3.4). These variables were calculated from the ratio values, relative to water (with α correction) and relative to Cr.

Table 3.4: E/I imbalance (median (IQR)) relative to water (W) (with α correction) and creatine (Cr) in the frontal lobe of Parkinson's Disease (PD), Huntington's Disease (HD) and control participants.

	PD	HD	Control	p-value
n	6	13	6	
$(\text{Glx/GABA})_{W(\alpha c)}$	3.97 (0.98)	3.44 (2.00)	2.75 (0.68)	0.275
$(\text{Glx/GABA})_{Cr}$	1.10 (0.26)	0.95 (0.55)	0.76 (0.19)	0.275

For the E/I imbalance (Table 3.4), Kruskal-Wallis tests showed no significant differences between groups for both ratios $(\text{Glx/GABA})_{W(\alpha c)}$: $H(2) = 2.58$, $p = 0.275$; $(\text{Glx/GABA})_{Cr}$: $H(2) = 2.58$, $p = 0.275$).

Given our main hypothesis that an E/I imbalance would exist, at least, between each clinical group and the controls, reflected on a difference in Glx/GABA ratios, the statistical power achieved on the previous analysis was calculated using G*Power. Given the sample size of each group and the $(\text{Glx/GABA})_{W(\alpha c)}$ (ratio of absolute α-corrected levels of Glx and GABA) means and standard deviation (Control: 3.22 ± 1.672; HD: 3.77 ± 1.227; PD: 3.84 ± 0.667) to calculate the effect size, we estimated the power achieved in our analysis, but performed as pairwise comparisons (for a Wilcoxon-Mann-Whitney test) between each clinical group and the control group. For HD vs. Controls, we achieved a power of 11%, and for PD vs. Controls we achieved a power of 12%. These results suggest that our analyses were underpowered given the small sample size after rejection of datasets during visual quality control check. Therefore it is very likely that data was insufficient to detect meaningful differences between groups.

At last, a *post-hoc* analysis was performed to calculate the number of subjects (minimum sample size) needed to detect differences on Glx/GABA ratios between each clinical group and Controls, as previously hypothesized. G*Power was again used to perform this estimation, based on our data, as preliminary data to estimate the effect sizes. Sample sizes were determined to achieve the referred effect sizes, with a power of 80%, considering a two-tailed significance level of 5%, using an

independent samples t-test. The estimated effect size, based on the mean values of $(\text{Glx/GABA})_{W(\alpha c)}$ (ratio of absolute values, α-corrected for tissue fraction) was 0.37 when comparing HD vs. Control groups and 0.49 when comparing PD vs. Control groups. The sample size (allocation ratio = 1) required to achieve these effect sizes, is 113/113 individuals (HD/Controls) and 68/68 individuals (PD/Controls).

3.3 Spectral quality assessment

Quality assessment of ^{1}H-MRS data is still under intense debate [47]. Apart from clearly defined artifacts, many issues cannot be easily detected, and some measures have been proposed to quantitatively evaluate data and fitting quality. Gannet provides some of these estimates to indirectly assess signal quality: Fit Errors (%), and both, FWHM (Hz) and SNR.

Data were only analyzed for the 25 participants that passed the visual quality control after loading and preprocessing of the edited MEGA-PRESS spectrum. The overall results are presented as boxplots for SNR in Figure 3.3, FWHM (Hz) in Figure 3.6, and Fit Errors (%) in Figure 3.11.

Kruskal-Wallis tests were carried out to compare model fitting parameters between both clinical groups, PD and HD, and Control groups.

SNR. Signal-to-noise ratio (SNR, $n = 25$) for GABA (median (IQR) = 29.5 (12.49)); Glx (median (IQR) = 31.1 (12.39)) and Water (median (IQR) = 23132.4 (3211.74)) signals were analyzed (Figure 3.3). Significant statistical differences were found between groups for Water SNR ($H(2) = 7.63$, $p = 0.022$, Figure 3.4c). *Post-hoc* pairwise tests with BH adjustment showed that Water signal SNR was significantly higher in PD comparing to HD group ($p = 0.014$). No differences were found for Water signal SNR between the Control group and any of the clinical groups. Regarding the SNR of the metabolites of interest signals, no significant statistical differences were found between groups (GABA: $H(2) = 0.25$, $p = 0.881$; Glx: $H(2) = 1.14$, $p = 0.565$). Since HD presents a wide variability of SNR for GABA and Glx signals, representative edited spectra with the highest and lowest SNR for both metabolites are shown in Figure 3.5.

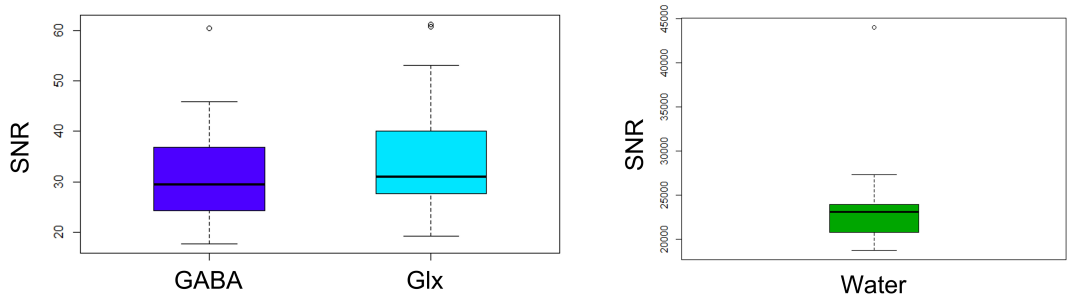

Figure 3.3: Distribution of SNR values for the remaining 25 participants (left) GABA and Glx, and (right) Water signals.

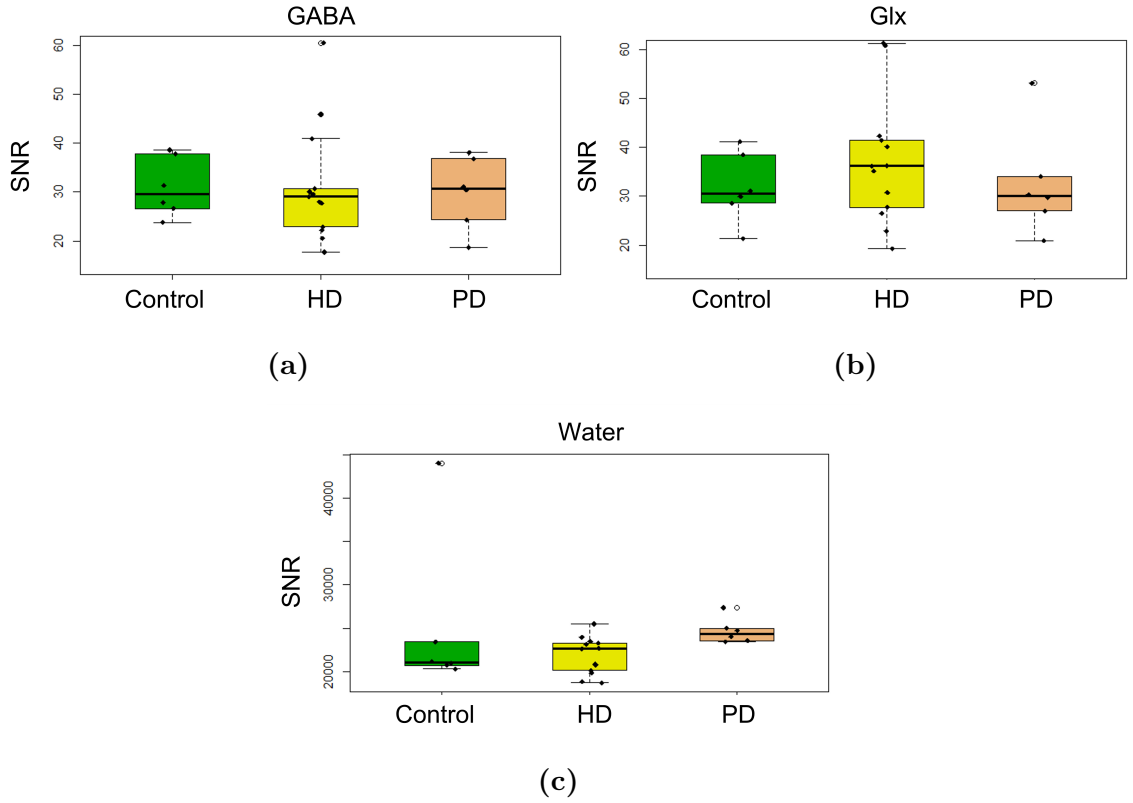

Figure 3.4: Distribution of SNR values for (a) GABA, (b) Glx and (c) Water signals of Parkinson's Disease (PD), Huntington's Disease (HD) and Control participants.

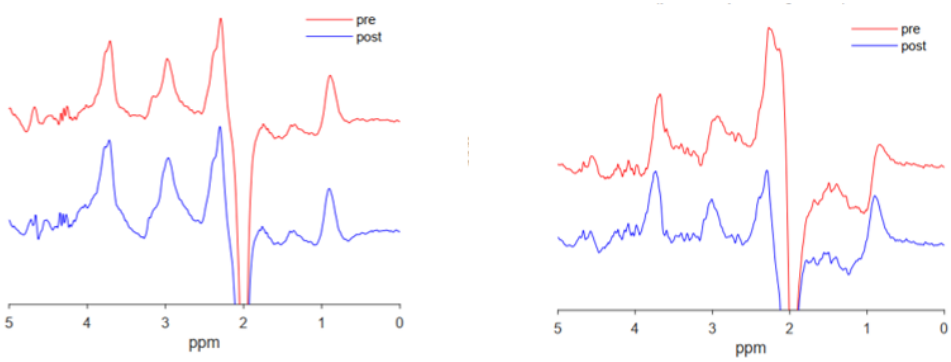

Figure 3.5: Representative edited spectra pre-alignment (red) and post-alignment (blue) of two HD patients with the (a) highest (male, 36y) and (b) lowest SNR (female, 47y) for both GABA and Glx signals.

FWHM. Full-width-at-half-maximum (FWHM (Hz), $n = 25$) as a measure of the linewidth for GABA (median (IQR) = 22.9 (4.28) Hz); Glx (median (IQR) = 22.9 (6.81) Hz), and Water (median (IQR) = 16.1 (2.93) Hz) peaks was evaluated (Figure 3.6). Kruskal-Wallis test showed a statistical significant difference between groups for FWHM of the Water peak ($H(2) = 7.33$, $p = 0.026$, Figure 3.7c). These differences were found between PD (lower) and Controls ($p = 0.013$), but not between the clinical groups (*post-hoc* pairwise tests with BH adjustment). There were no differences between groups for FWHM values of GABA ($H(2) = 2.18$, $p = 0.336$), and Glx peaks ($H(2) = 0.29$, $p = 0.866$). For visualization purposes, representative edited spectra and corresponding model fitting for GABA and Glx are shown in Figure 3.8 and Figure 3.9, respectively.

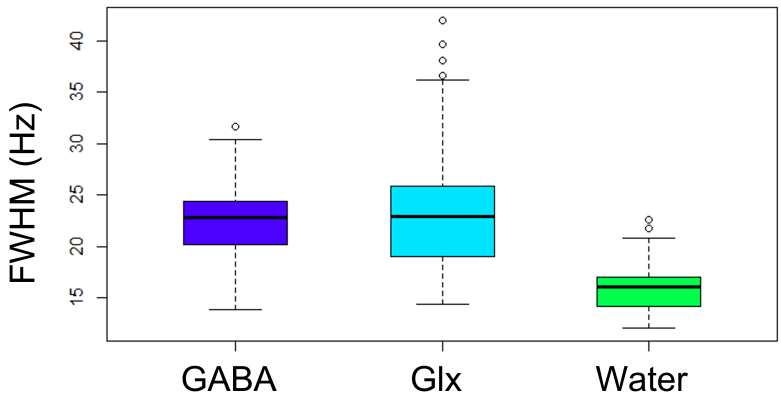

Figure 3.6: Distribution of FWHM (Hz) values of GABA, Glx and Water peaks from the final cohort of 25 participants.

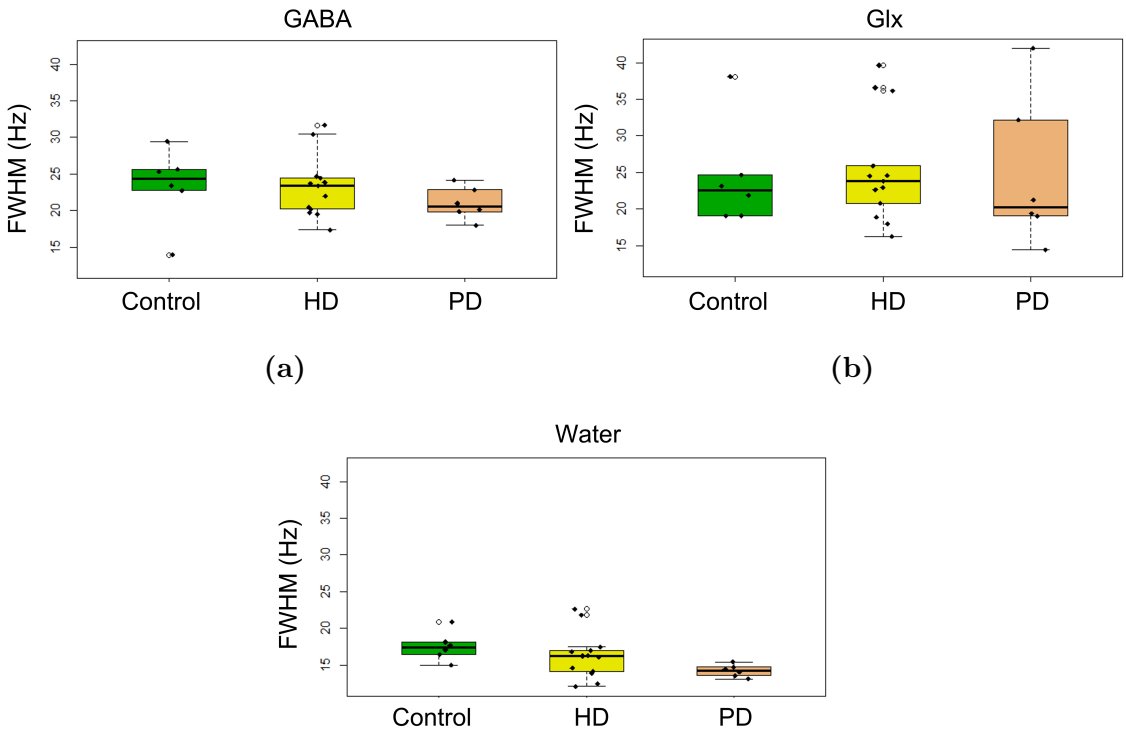

Figure 3.7: Distribution of FWHM values (Hz) of (a) GABA, (b) Glx and (c) Water signals in Parkinson's Disease (PD), Huntington's Disease (HD) and Control groups.

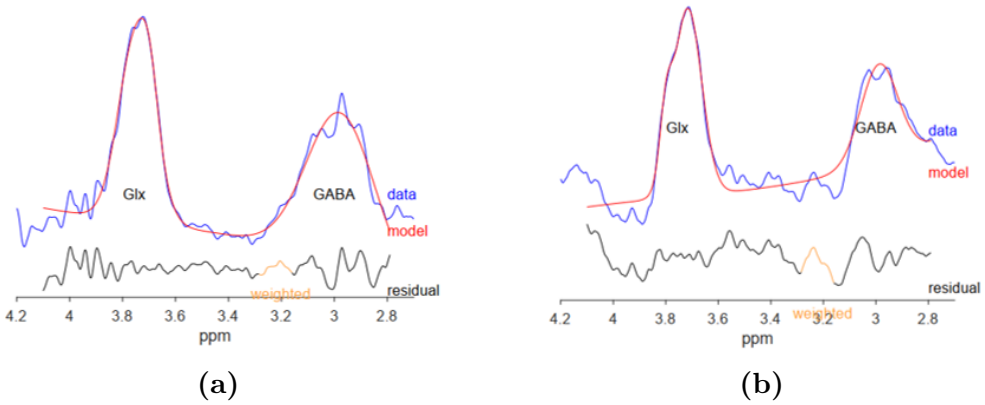

Figure 3.8: Representative edited spectra (blue) and model fitting (red) of two HD patients with the (a) largest (female, 25y), and (b) smallest (male,41y) GABA signal FWHM.

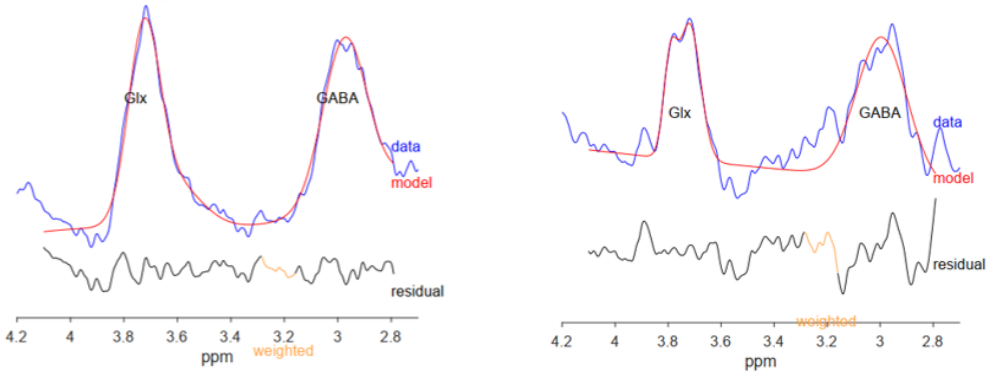

(a) **(b)**

Figure 3.9: Representative edited spectra (blue) and model fitting (red) of two HD patients with the (a) largest (female, 47y), and (b) smaller (female, 52y) Glx peak FWHM.

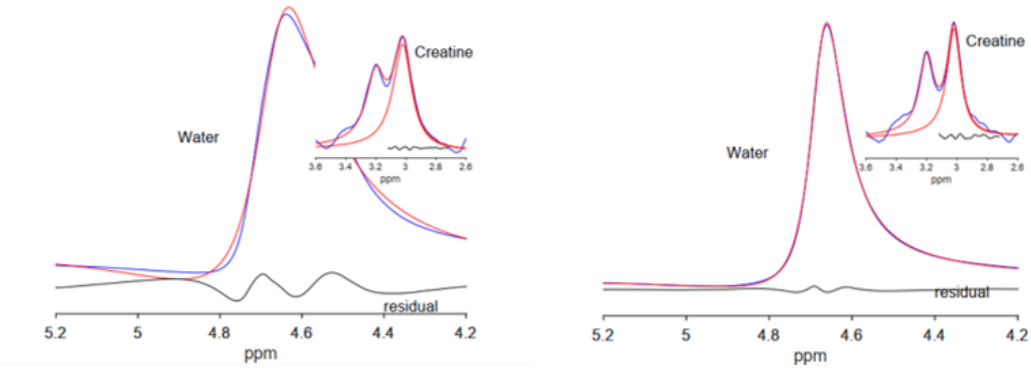

(a) **(b)**

Figure 3.10: Representative peak fitting of used reference signals (Water and Creatine) of two HD patients with the (a) largest (female, 25y), and (b) smaller (female, 52y) water signal FWHM (Hz).

Fit Errors. After modeling the fits of the metabolites, Gannet estimates the corresponding Fit Errors (%) as the standard deviation of the metabolite peak fit residual expressed as a percentage of the amplitude of the modeled metabolite peak. Overall fit errors (metabolites relative to Water and to Creatine) were evaluated as a combined Fit Error (Methods section, Equation 2.3). One PD case and one Control presented extreme metabolites/Cr Fit Errors (FitError GABA/Cr: 669.9% (PD) and 1393.5% (Control); FitError Glx/Cr: 669.9% (PD) and 1393.5% (Control)) due to complete failure of the Creatine signal fitting. The values of these variables for the two cases were removed from the following analysis on Fit Errors. These overall Fit Errors for the final sample (Figure 3.11) were in the 3-11% range (GABA/W: n = 25, median = 5.6%; Glx/W: n = 25, median = 4.9%; GABA/Cr: n = 23,

median = 5.8%; Glx/Cr: n = 23, median = 4.9%). Kruskal-Wallis tests showed no statistically significant differences of combined Fit Errors of GABA or Glx (Figure 3.12) with both Water (GABA/W: $H(2) = 3.36$, $p = 0.186$); Glx/W: $H(2) = 1.67$, $p = 0.434$), and Creatine (GABA/Cr: $H(2) = 3.86$, $p = 0.145$; Glx/Cr: $H(2) = 4.12$, $p = 0.127$).

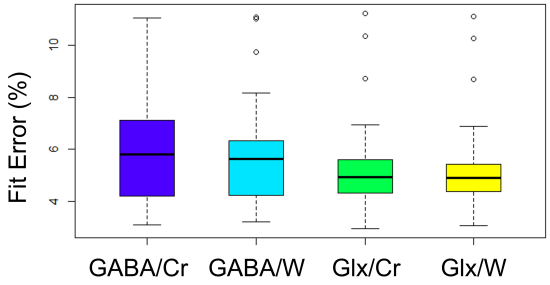

Figure 3.11: Distribution of the combination of GABA and creatine (GABA/Cr, n=23), GABA and water (GABA/W, n=25), Glx and creatine (Glx/Cr, n=23) and Glx and water (Glx/W, n=25) fit errors.

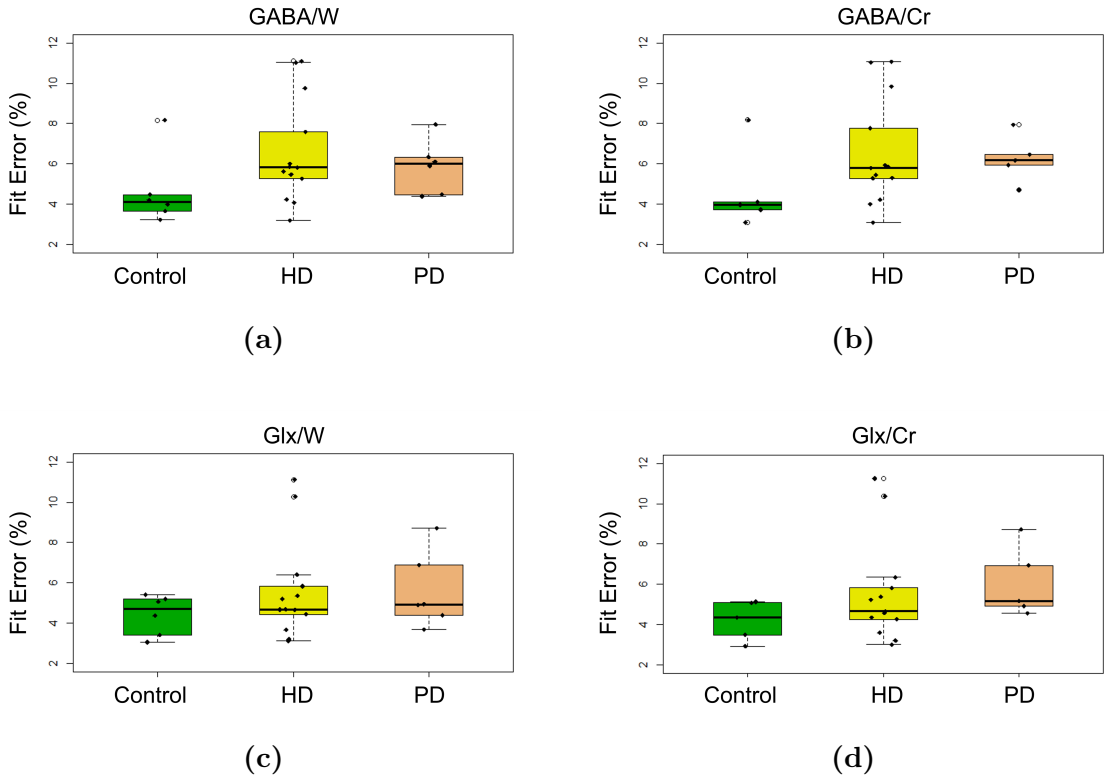

Figure 3.12: Distribution of combined Fit error values (%) in Parkinson's Disease (PD), Huntington's Disease (HD) and Control groups for: (a) GABA and Water (GABA/W), (b) GABA and Creatine (GABA/Cr, n = 5 for PD and n = 5 for Controls), (c) Glx and Water (Glx/W), (d) Glx and Creatine (Glx/Cr, n = 5 for PD and n = 5 for Control).

4

Discussion

In this work, we aimed to investigate the hypothesis that GABA and Glx levels are impaired in patients suffering from movement disorders. To achieve this goal, we measured, *in vivo*, levels of GABA and Glx in the frontal lobe of patients with Huntington's Disease (HD), Parkinson's Disease (PD), and a control group using proton Magnetic Resonance Spectroscopy (^{1}H-MRS).

Regarding demographic data (Table 3.1), some particular issues can be noted, which pose a challenge to direct group comparisons: the mean age of HD patients is lower than that of the PD patients, yet HD patients have had the disease for longer than PD patients. This is in accordance with both diseases' characteristics: HD commonly manifests earlier than PD. Nevertheless, we took into account these potential confounds.

We hypothesized that in early stages of PD, as we have in our cohort, frontal lobe dysfunctions, which are assumed to reflect cortical deafferentation relative to the striatal dopamine reduction [51], should be reflected on the GABA and Glx levels.

GABA and glutamate concentrations are known to vary with sex and age [25, 52]. Since both sex and age showed no statistically significant differences between groups in our final cohort, after the inspection of preprocessed edited spectra, we conclude we do have gender- and age-matched participants. Additionally, no statistically significant differences were found for any variable in the final cohort, which offered no limitations to further analysis. Guaranteeing age-matched participants was important not only for the reason stated above but also because aging influences the macromolecular contribution onto the GABA signal [31]. Therefore, a possible confound was avoided, since group studies comparing patients with controls, as ours, could be affected by macromolecular changes between groups.

Our first inspection of the collected data was through Gannet with the four main pre-processing steps. With the qualitative visual quality control assessment, we dis-

carded 44 participants mainly due to reasons previously stated in Methods section. Due to the fact the spectra presented so many issues since the beginning, this work will specially be focused on discussing the quality of the spectroscopy signal acquired and its impact on clinical studies of neurodegenerative disorders.

We analyzed data quality through some quantitative metrics such as FWHM, SNR and Fit Errors. Fit Errors (Figures 3.11 and 3.12) were expected to be small, since visual quality control was performed before fitting, and bad spectra were discarded. These values varied between 2.9% and 11.2%, which are acceptable values [53]. On the other hand, spectral linewidth, expressed as FWHM varied from 13.9Hz to 31.6Hz (GABA), suggesting poorly resolved peaks with metabolites overlap, leading to GABA fitting inaccuracies and estimates [47]. As expected, SNR values for water were much higher than the ones of metabolites, since water has a well-resolved peak, easily modeled in the unsuppressed signal. Whilst not the best SNR, the values for GABA are consistent with the literature [54]. Having a high SNR was desirable, as an attempt to discriminate the real MRS signal from the background noise. It would be possible to improve our SNR with longer scan times [47], but longer scanner times would contribute to other artifacts due to potential patients' motion. Other option would be to acquire a larger region of interest. For MEGA-PRESS, the typical voxel size is 3x3x3 cm^3 to compensate for the low SNR for GABA signal without compromising localization [31]. These issues are further examined in the next paragraphs, as well as related aspects in our analysis.

During the acquisition, monitorization of the participants by the radiographer occurred. The person responsible to acquire the images would take notes on whether the patient moved too much or not. The problem with this is that our voxel was still voluminous, and any minor movement observed, and even undetected movements with the naked eye, could have a huge impact in the acquisition and be responsible for detected artifacts. This person was also responsible for making sure that the voxel was properly placed [47]. This implies that there is the possibility of operator dependence.

Problems with the quality of the signals acquired can be often related with the fact that the patients under study have motor symptoms, precluding them from avoiding motion for the entire time of the data acquisition. In fact, this study was part of a bigger Project, in which MRS was performed after functional MRI (fMRI) runs, potentiating movement during MRS signal acquisition. Also, the voxel positioning was often challenging due to its dimensions, especially for HD patients in whom the atrophy commonly extends beyond the striatum to other subcortical and

also cortical structures such as the frontal cortex with the disease progression [55]. Even minor motion events are critical in MRS since these are not easily detected and may lead data recording in inaccurate voxel localizations, contamination from outer volume lipids, bone and/or ventricles, lower SNR and estimation errors [47]. Even if the signal is quantifiable, abnormalities resultant from voxel misplacement may be erroneously attributed to disease [47]. The fact that we performed a MEGA-PRESS without water suppression may have helped to minimize the effects of motion noise [23], but it still was not enough to improve all the spectra acquired. Moreover, the preceding fMRI acquisitions may have induced gradient-induced frequency drifts on MRS signal [56]. Even with the postprocessing these frequency drifts may have caused some subtraction artifacts and impacting metabolites estimation.

Other advantages of acquiring unsuppressed water spectra could be enumerated: it can offer an internal reference for metabolites estimation; it allows for frequency drifts and eddy-current correction; signals with small chemical shift differences relative to water resonance can be more accurately detected since they could be suppressed by water suppression pulses; RF pulses used for water suppression increase the total RF power deposition and, in some water suppression methods, they may even cause magnetization transfer, which could lead to systematic errors in metabolite quantification; water suppression may present phase and lineshape distortions in the spectrum if the water signal is incompletely suppressed, and since it is unsuppressed this should not happen [23, 57].

Our data was acquired a few years back and since then some improvements have occurred in this field, not only related to hardware and software upgrades, but also with acquisition techniques. One example is the fact that our data was saved as Siemens RDA files. Now, it is possible to export raw MRS data in TWIX format. Whereas RDA saves time-averaged ON and OFF files, TWIX contains each individual spectrum, allowing to detect and exclude or down weight bad averages, reducing its contribution to the final average file, and allowing the application of more several postprocessing approaches than RDA files [47]. Another example, regarding hardware updates, consists in increasing the number of channels in the head coil used (from a 12-channel head coil to a 20-channel head coil, for example) to improve the quality of the signal, as increasing the number of channels increases SNR [58].

In line with the main objective of this study, GABA and Glx concentrations relative to water and corrected for tissue fractions were estimated and compared between both clinical groups (HD and PD) and Controls (Table 3.3 and Figure 3.1). Ratios of GABA and Glx relative to Water (uncorrected) and to Creatine (also available

in Table 3.3 and Figure 3.1) were also evaluated. When using water as a concentration reference for MRS, as we did, it is important to acknowledge some aspects. An accurate correction for partial volume effects within the voxel, that often occur when multiple tissues contribute to a single voxel, impacting in intensities at tissue boundaries, is especially important when performing group comparisons and correlations with other parameters. Therefore, in this work, tissue segmentation was performed to estimate GM, WM and CSF fractions enclosed in the voxel. Moreover, when correcting for water content, it is recommended to include measures of apparent water density and relaxivity in GM, WM and CSF in the metabolite estimation algorithm [45, 59]. Therefore, metabolites (GABA and Glx) levels relative to water with tissue correction were considered the most robust variables to analyze E/I balance in these groups.

Regarding tissue segmentation statistics (Table 3.2), a significant between group difference was found for CSF (%), with the statistically significant differences occurring between Controls and both PD and HD. This was expected, since relative increase of the CSF compartment is expected with cerebral atrophy [45].

Another possible limitation to our study, inherent to the methods used, is the fact that we are calculating ratios and not actual concentrations. Therefore, we ended up using approximations to measure GABA and Glx, which we later used to calculate the ratio Glx/GABA. Using ratios to Cr can also have further implications: if both Cr and metabolite are decreased, for example, the ratio will show no alterations that could otherwise actually be relevant. Additionally, denominators with inaccurate values, which was the case with Cr in our study, will lead to abnormal variances in the metabolite ratios [60]. At this point, it is important to remind that the GABA signal referred throughout this study is in fact contaminated with co-edited macromolecules and homocarnosine signals. Moreover, Glx corresponds to a pool of glutamate and glutamine. Thus the E/I imbalance in the brain is being assessed through two potentially confounded measures.

Since, in some subjects, ratios to Creatine showed incorrect estimations due to modeling and estimation failures, we will refrain from discussing them further. Observing the boxplots (Figure 3.1) for the metabolites levels, as well as the table (Table 3.3), the median of GABA relative to Water (corrected) was lower for the clinical groups when comparing to Controls, especially for HD group. On the other hand, median of Glx relative to Water (corrected) is higher for the clinical groups when comparing to Controls, particularly for HD group.

A previous study with GABA-edited MEGA-PRESS data, showed a significant in-

crease in GABA levels (but not Glx) in the basal ganglia of PD patients (n = 20) when comparing to controls (n = 17) [16]. Meanwhile, in the left prefrontal cortex, higher levels (but not statistically significant) of both GABA and Glx were found [16]. Despite the low rate of dropouts, the authors did not mention any quality control for the spectra, which raises concerns of bias due to possible inadequate participant inclusions. In the work of Adanyeguh *et al.* (2018), Glutamate and GABA levels were assessed with a modified short-TE semi-LASER (LASER, Localization by Adiabatic Selective Refocusing) ^{1}H-MRS approach in the striatum and the visual cortex (only Glx was analyzed) of 10 HD patients and 10 controls [61]. Opposite to the trends found in our study, significantly lower concentrations of Glutamate were found in HD patients on the striatum (9 patients), but no GABA differences were found. In the visual cortex, no changes in Glutamate were found [61]. In another study, 12 early stage or premanifest HD patients and 12 age-matched healthy controls underwent 7T to acquire ^{1}H-MRS data in a 7.2ml voxel in the posterior cingulate cortex using STEAM sequence [62]. Significantly lower glutamate levels were found in HD patients when compared to controls, but not for GABA estimates. This lack of replication can be due to several reasons: heterogeneity of PD and HD syndromes, differences in acquisition methods (magnet strength, localization and suppression sequences applied, shimming, etc.), voxel sizes and locations, differences in processing steps (quality constraints, modeling approaches and algorithms, etc.) and/or statistical power.

We do hypothesize that the trends on both GABA and Glx levels between groups that we found are not statistically significant possibly due to underpowered analysis. In fact, our sample size diminished considerably from the expected. Initially, data was collected from 70 participants, a more robust sample size. However, after visual inspection, only 25 datasets were analyzed due to low quality of the signal. The achieved power of the statistical analysis for the final sample was indeed very low leading to unclear conclusions. Even though not commonly mentioned in the literature, dropouts' rate can be a critical issue and future studies similar to this should keep this in consideration when designing the experimental protocol and estimating sample sizes.

5

Conclusion and Future Work

This exploratory study gives insight on how challenging examining brain metabolites *in vivo* can be, especially when targeting low-concentration metabolites such as GABA in neurodegenerative movement disorders such as Parkinson's and Huntington's Disease. Importantly, study design and data acquisition and analysis methodologies are critical concerns and should be carefully deliberated, especially due to motion artifacts that are practically unavoidable in these cohorts and will degrade the MRS signal leading to inaccurate estimates.

After a qualitative visual quality control inspection of the edited spectra, nearly 63% of datasets were discarded. Literature often disregards or does not report quality assessment procedures and/or the dropout rate prior to fitting that may lead to underpowered conclusions. This is very important because some of the previously reported findings may be derived from systematic artefactual biases. In our case, some of the potential factors that contributed to the high rate of excluded datasets can be associated with: *head motion* - patients under study have movement disorders, and motion deeply affects the quality of the signal; *voxel size* – larger voxels are difficult to fit without having contamination from unwanted areas such as air, bone, ventricles, etc.; *voxel localization* – the frontal lobe is a difficult region to perform spectroscopy due to the difference on air/brain susceptibility that causes magnetic field distortions, leading to a poorer spectral quality [63]; *protocol design* – performing MRS at the end of the experiment may potentiate the occurrence of motion artifacts and also frequency drifts due to gradients; etc. Recently, experts on proton MRS have gathered some recommendations to improve ^{1}H-MRS practices in data acquisition, analysis, and reporting [64, 65] to increase reproducibility and quality assurance.

It will be certainly possible to determine the impact of movement in the quality of the spectra, and even quantify it, with the advance of technology and the development of new correction algorithms to be applied both during and/or after acquisition, with-

out the need for subject immobilization. Experiments aiming to calculate dropout rate, through registration of motion that can be related to the quality of the spectra, would be possible future work to be done in this field. The implementation of motion correction procedures is strongly advised and MRS groups have been focused on the development of new strategies [66]. Motion effects could be partially mitigated through the implementation of algorithms that are able to detect movement and correct the voxel position both prospectively and ideally on-line, with tracking methods [67], but that would need to be implemented by the scanner vendor in its equipment, in this case Siemens. A suggestion envisioning better quality control, would be a more automated and real-time system for artifact detection and correction integrated in the image scanner, since *post-hoc* offline corrections will not be able to fully correct wrong spatial measurements.

Others, have nevertheless suggested retrospective approaches to be implemented in post-processing steps, focusing on frequency shifts induced by motion and phasing corrections [68], along with rejection of motion corrupted transients [66]. To do so, TWIX data are a considerable upgrade since MRS data are stored as the collection of individual transients allowing for more robust post-processing methods and allowing to selectively discard the corrupted slices [64]. However, this does not allow to correct measurements from wrong locations which may lead to partial volume errors.

Despite the trends found for metabolites levels differences between groups, the results were not statistically significant. Yet, given that our sample sizes were harshly diminished due to our quality constraints, we do believe that some effects may be concealed by an underpowered analysis. Moreover, GABA signal was not pure, and new approaches on GABA estimation with macromolecules suppression should be considered in new studies [69,70]. In addition, our voxel size was substantially large. In the future, using a scanner with a higher field strength of 7T, for example, would allow using a smaller voxel volume, which would allow for a better defined region of interest, less prone to partial volume effects.

To conclude, despite not having found GABA and Glx levels differences between groups, this exploratory study (that was part of a bigger project) helped raise attention for several issues that are highly critical when studying neurodegenerative movement disorders. The most fundamental problem detected was the motion artifacts that consequently lead to a high dropout rate of spectra. We hope that this study has given future researchers a better understanding of the existing problems and offered some solutions to bypass most of the issues we faced during data acquisition and analysis. Criteria for spectral quality assessment must be evaluated and

robust consensual metrics are needed to achieve full reproducibility.

References

[1] W. Poewe, K. Seppi, C. M. Tanner, G. M. Halliday, P. Brundin, J. Volkmann, A.-E. Schrag, and A. E. Lang, "Parkinson disease," *Nature reviews Disease primers*, vol. 3, no. 1, pp. 1–21, 2017.

[2] T. Hoang, S. Bluml, D. Dubowitz, R. Moats, O. Kopyov, D. Jacques, and B. Ross, "Quantitative proton-decoupled ^{31}p mrs and ^{1}h mrs in the evaluation of huntington's and parkinson's diseases," *Neurology*, vol. 50, no. 4, pp. 1033–1040, 1998.

[3] E. Fonoff, "Levodopa, a medicação que revolucionou o tratamento da doença de parkinson." `https://www.erichfonoff.com.br/blog/levodopa-a-medicacao-que-revolucionou-o-tratamento-de-parkinson/`. [Online; accessed 29-June-2021].

[4] J. Jankovic, "Parkinson's disease: clinical features and diagnosis," *Journal of neurology, neurosurgery & psychiatry*, vol. 79, no. 4, pp. 368–376, 2008.

[5] D. K. Khatri, M. Choudhary, A. Sood, and S. B. Singh, "Anxiety: An ignored aspect of parkinson's disease lacking attention," *Biomedicine Pharmacotherapy*, vol. 131, p. 110776, 2020.

[6] R. Bhidayasiri and D. D. Truong, "Motor complications in parkinson's disease: clinical manifestations and management," *Journal of the neurological sciences*, vol. 266, no. 1-2, pp. 204–215, 2008.

[7] S. Broeder, E. Nackaerts, K. Cuypers, R. Meesen, G. Verheyden, and A. Nieuwboer, "tdcs-enhanced consolidation of writing skills and its associations with cortical excitability in parkinson disease: a pilot study," *Neurorehabilitation and neural repair*, vol. 33, no. 12, pp. 1050–1060, 2019.

[8] B. Elahi, B. Elahi, and R. Chen, "Effect of transcranial magnetic stimulation on parkinson motor function—systematic review of controlled clinical trials,"

Movement Disorders, vol. 24, no. 3, pp. 357–363, 2009.

[9] P. Morrish, G. Sawle, and D. Brooks, "Regional changes in [^{18}f]-dopa metabolism in the striatum in parkinson's disease," *Brain*, vol. 119, no. 6, pp. 2097–2103, 1996.

[10] G. Huntington, "On chorea," *Med Surg Rep*, no. 26, pp. 317–321, 1872.

[11] R. A. Roos, "Huntington's disease: a clinical review," *Orphanet journal of rare diseases*, vol. 5, no. 1, pp. 1–8, 2010.

[12] G. P. Bates, R. Dorsey, J. F. Gusella, M. R. Hayden, C. Kay, B. R. Leavitt, M. Nance, C. A. Ross, R. I. Scahill, R. Wetzel, *et al.*, "Huntington disease," *Nature reviews Disease primers*, vol. 1, no. 1, pp. 1–21, 2015.

[13] S. Blumenstock and I. Dudanova, "Cortical and striatal circuits in huntington's disease," *Frontiers in neuroscience*, vol. 14, p. 82, 2020.

[14] S. E. Purdon, E. Mohr, V. Ilivitsky, and B. Jones, "Huntington's disease: pathogenesis, diagnosis and treatment," *Journal of Psychiatry and Neuroscience*, vol. 19, no. 5, p. 359, 1994.

[15] D. Victorson, N. E. Carlozzi, S. Frank, J. L. Beaumont, W. Cheng, B. Gorin, M. S. Duh, D. Samuelson, D. Tulsky, S. Gutierrez, *et al.*, "Identifying motor, emotional - behavioral, and cognitive deficits that comprise the triad of hd symptoms from patient, caregiver, and provider perspectives," *Tremor and Other Hyperkinetic Movements*, vol. 4, 2014.

[16] R. L. O'Gorman Tuura, C. R. Baumann, and H. Baumann-Vogel, "Beyond dopamine: Gaba, glutamate and the axial symptoms of parkinson disease," *Frontiers in neurology*, vol. 9, p. 806, 2018.

[17] C. M. Henstridge, M. Tzioras, and R. C. Paolicelli, "Glial contribution to excitatory and inhibitory synapse loss in neurodegeneration," *Frontiers in cellular neuroscience*, vol. 13, p. 63, 2019.

[18] B. S. Meldrum, "Glutamate as a neurotransmitter in the brain: review of physiology and pathology," *The Journal of nutrition*, vol. 130, no. 4, pp. 1007S–1015S, 2000.

[19] Y. Zhou and N. C. Danbolt, "Glutamate as a neurotransmitter in the healthy brain," *Journal of neural transmission*, vol. 121, no. 8, pp. 799–817, 2014.

[20] M. van der Graaf, "*In vivo* magnetic resonance spectroscopy: basic methodology and clinical applications," *European Biophysics Journal*, vol. 39, no. 4, pp. 527–540, 2010.

[21] R. A. Pooley, "Fundamental physics of mr imaging," *Radiographics*, vol. 25, no. 4, pp. 1087–1099, 2005.

[22] J. M. Tognarelli, M. Dawood, M. I. Shariff, V. P. Grover, M. M. Crossey, I. J. Cox, S. D. Taylor-Robinson, and M. J. McPhail, "Magnetic resonance spectroscopy - principles and techniques: lessons for clinicians," *Journal of clinical and experimental hepatology*, vol. 5, no. 4, pp. 320–328, 2015.

[23] Z. Dong, "Proton mrs and mrsi of the brain without water suppression," *Progress in nuclear magnetic resonance spectroscopy*, vol. 86, pp. 65–79, 2015.

[24] N. A. Puts and R. A. Edden, "*In vivo* magnetic resonance spectroscopy of gaba: a methodological review," *Progress in nuclear magnetic resonance spectroscopy*, vol. 60, p. 29, 2012.

[25] M. Castillo, L. Kwock, and S. K. Mukherji, "Clinical applications of proton mr spectroscopy," *American journal of neuroradiology*, vol. 17, no. 1, pp. 1–15, 1996.

[26] C. D. Rae, "A guide to the metabolic pathways and function of metabolites observed in human brain ^{1}h magnetic resonance spectra," *Neurochemical research*, vol. 39, no. 1, pp. 1–36, 2014.

[27] T. Liu, Y. Wang, S. Zhong, B. Wang, X. Liao, S. Lai, and Y. Jia, "A comparison of neurometabolites between remitted bipolar disorder and depressed bipolar disorder: a proton magnetic resonance spectroscopy study," *Journal of affective disorders*, vol. 211, pp. 153–161, 2017.

[28] R. A. Edden and P. B. Barker, "Spatial effects in the detection of γ-aminobutyric acid: Improved sensitivity at high fields using inner volume saturation," *Magnetic Resonance in Medicine: An Official Journal of the International Society for Magnetic Resonance in Medicine*, vol. 58, no. 6, pp. 1276–1282, 2007.

[29] K. Landheer, R. F. Schulte, M. S. Treacy, K. M. Swanberg, and C. Juchem, "Theoretical description of modern ^{1}h *in vivo* magnetic resonance spectroscopic pulse sequences," *Journal of Magnetic Resonance Imaging*, vol. 51, no. 4, pp. 1008–1029, 2020.

[30] I.-Y. Choi, O. C. Andronesi, P. Barker, W. Bogner, R. A. Edden, L. G. Kaiser, P. Lee, M. Marjańska, M. Terpstra, and R. A. de Graaf, "Spectral editing in ^{1}h magnetic resonance spectroscopy: Experts' consensus recommendations," *NMR in Biomedicine*, vol. 34, no. 5, p. e4411, 2021.

[31] P. G. Mullins, D. J. McGonigle, R. L. O'Gorman, N. A. Puts, R. Vidyasagar, C. J. Evans, R. A. Edden, *et al.*, "Current practice in the use of mega-press spectroscopy for the detection of gaba," *Neuroimage*, vol. 86, pp. 43–52, 2014.

[32] K. L. Chan, N. A. Puts, M. Schär, P. B. Barker, and R. A. Edden, "Hermes: Hadamard encoding and reconstruction of mega-edited spectroscopy," *Magnetic resonance in medicine*, vol. 76, no. 1, pp. 11–19, 2016.

[33] F. Júlio, M. J. Ribeiro, A. Morgadinho, M. Sousa, M. van Asselen, M. R. Simões, M. Castelo-Branco, and C. Januário, "Cognition, function and awareness of disease impact in early parkinson's and huntington's disease," *Disability and Rehabilitation*, pp. 1–19, 2020.

[34] F. Júlio, M. J. Ribeiro, M. Patrício, A. Malhão, F. Pedrosa, H. Gonçalves, M. Simões, M. van Asselen, M. R. Simões, M. Castelo-Branco, *et al.*, "A novel ecological approach reveals early executive function impairments in huntington's disease," *Frontiers in psychology*, vol. 10, p. 585, 2019.

[35] G. E. Alexander, M. R. DeLong, and P. L. Strick, "Parallel organization of functionally segregated circuits linking basal ganglia and cortex," *Annual review of neuroscience*, vol. 9, no. 1, pp. 357–381, 1986.

[36] U. Klose, "*In vivo* proton spectroscopy in presence of eddy currents," *Magnetic resonance in medicine*, vol. 14, no. 1, pp. 26–30, 1990.

[37] "Finally! it's here - universal edited mrs." `http://www.gabamrs.com/blog/2019/2/16/finally-its-here-universal-standardized-edited-mrs`, 2019. [Online; accessed 22-July-2021].

[38] O. C. d'Almeida, I. R. Violante, B. Quendera, and M. Castelo-Branco, "Mitochondrial pathophysiology beyond the retinal ganglion cell: occipital gaba is decreased in autosomal dominant optic neuropathy," *Graefe's Archive for Clinical and Experimental Ophthalmology*, vol. 256, no. 12, pp. 2341–2348, 2018.

[39] J. F. Jansen, W. H. Backes, K. Nicolay, and M. E. Kooi, "^{1}h mr spectroscopy of the brain: absolute quantification of metabolites," *Radiology*, vol. 240, no. 2, pp. 318–332, 2006.

[40] B. S. Li, H. Wang, and O. Gonen, "Metabolite ratios to assumed stable creatine level may confound the quantification of proton brain mr spectroscopy," *Magnetic resonance imaging*, vol. 21, no. 8, pp. 923–928, 2003.

[41] R. A. Edden, N. A. Puts, A. D. Harris, P. B. Barker, and C. J. Evans, "Gannet: A batch-processing tool for the quantitative analysis of gamma-aminobutyric acid-edited mr spectroscopy spectra," *Journal of Magnetic Resonance Imaging*, vol. 40, no. 6, pp. 1445–1452, 2014.

[42] M. Mikkelsen, "Tissue Correction." `https://markmikkelsen.github.io/Gannet-docs/tissue-correction.html`, 2020. [Online; accessed 22-September-2021].

[43] J. Ashburner and K. J. Friston, "Unified segmentation," *Neuroimage*, vol. 26, no. 3, pp. 839–851, 2005.

[44] "Gannet 3.1 released." `http://www.gabamrs.com/blog/2019/6/18/gannet-31-released`, 2019. [Online; accessed 20-July-2021].

[45] A. D. Harris, N. A. Puts, and R. A. Edden, "Tissue correction for gaba-edited mrs: Considerations of voxel composition, tissue segmentation and tissue relaxations," *Journal of Magnetic Resonance Imaging*, vol. 42, no. 5, pp. 1431–1440, 2015.

[46] M. Mikkelsen, S. Tapper, J. Near, S. H. Mostofsky, N. A. Puts, and R. A. Edden, "Correcting frequency and phase offsets in mrs data using robust spectral registration," *NMR in Biomedicine*, vol. 33, no. 10, p. e4368, 2020.

[47] R. Kreis, "Issues of spectral quality in clinical ^{1}h-magnetic resonance spectroscopy and a gallery of artifacts," *NMR in Biomedicine*, vol. 17, no. 6, pp. 361–381, 2004.

[48] RStudio Team, *RStudio: Integrated Development Environment for R*. RStudio, PBC, Boston, MA, 2021.

[49] F. Faul, E. Erdfelder, A.-G. Lang, and A. Buchner, *G*Power 3: A flexible sta-tistical power analysis program for the social, behavioral, and biomedical sciences*. Behavior Research Methods, 2007.

[50] P. J. Pouwels and J. Frahm, "Regional metabolite concentrations in human brain as determined by quantitative localized proton mrs," *Magnetic resonance in medicine*, vol. 39, no. 1, pp. 53–60, 1998.

[51] R. de la Fuente-Fernández, "Frontostriatal cognitive staging in parkinson's disease," *Parkinson's Disease*, vol. 2012, 2012.

[52] R. L. O'Gorman, L. Michels, R. A. Edden, J. B. Murdoch, and E. Martin, "In vivo detection of gaba and glutamate with mega-press: reproducibility and gender effects," *Journal of magnetic resonance imaging*, vol. 33, no. 5, pp. 1262–1267, 2011.

[53] N. A. Puts, S. Heba, A. D. Harris, C. J. Evans, D. J. McGonigle, M. Tegenthoff, T. Schmidt-Wilcke, and R. A. Edden, "Gaba levels in left and right sensorimotor cortex correlate across individuals," *Biomedicines*, vol. 6, no. 3, p. 80, 2018.

[54] M. Mikkelsen, P. B. Barker, P. K. Bhattacharyya, M. K. Brix, P. F. Buur, K. M. Cecil, K. L. Chan, D. Y.-T. Chen, A. R. Craven, K. Cuypers, *et al.*, "Big gaba: Edited mr spectroscopy at 24 research sites," *Neuroimage*, vol. 159, pp. 32–45, 2017.

[55] B. Tan, R. Shishegar, G. R. Poudel, A. Fornito, and N. Georgiou-Karistianis, "Cortical morphometry and neural dysfunction in huntington's disease: A review," *European Journal of Neurology*, vol. 28, no. 4, pp. 1406–1419, 2021.

[56] A. D. Harris, B. Glaubitz, J. Near, C. John Evans, N. A. Puts, T. Schmidt-Wilcke, M. Tegenthoff, P. B. Barker, and R. A. Edden, "Impact of frequency drift on gamma-aminobutyric acid-edited mr spectroscopy," *Magnetic resonance in medicine*, vol. 72, no. 4, pp. 941–948, 2014.

[57] I. Tkáč, D. Deelchand, W. Dreher, H. Hetherington, R. Kreis, C. Kumaragamage, M. Považan, D. M. Spielman, B. Strasser, and R. A. de Graaf, "Water and lipid suppression techniques for advanced ^{1}h-mrs and mrsi of the human brain: experts' consensus recommendations," *NMR in Biomedicine*, vol. 34, no. 5, p. e4459, 2021.

[58] T. Schmitt and J. W. Rieger, "Recommendations of choice of head coil and prescan normalize filter depend on region of interest and task," *Frontiers in Neuroscience*, vol. 15, p. 1349, 2021.

[59] C. Gasparovic, T. Song, D. Devier, H. J. Bockholt, A. Caprihan, P. G. Mullins, S. Posse, R. E. Jung, and L. A. Morrison, "Use of tissue water as a concentration reference for proton spectroscopic imaging," *Magnetic Resonance in Medicine: An Official Journal of the International Society for Magnetic Resonance in Medicine*, vol. 55, no. 6, pp. 1219–1226, 2006.

[60] M. Wilson, O. Andronesi, P. B. Barker, R. Bartha, A. Bizzi, P. J. Bolan, K. M. Brindle, I.-Y. Choi, C. Cudalbu, U. Dydak, *et al.*, "Methodological consensus on clinical proton mrs of the brain: review and recommendations," *Magnetic resonance in medicine*, vol. 82, no. 2, pp. 527–550, 2019.

[61] I. M. Adanyeguh, M.-L. Monin, D. Rinaldi, L. Freeman, A. Durr, S. Lehéricy, P.-G. Henry, and F. Mochel, "Expanded neurochemical profile in the early stage of huntington disease using proton magnetic resonance spectroscopy," *NMR in Biomedicine*, vol. 31, no. 3, p. e3880, 2018.

[62] P. G. Unschuld, R. A. Edden, A. Carass, X. Liu, M. Shanahan, X. Wang, K. Oishi, J. Brandt, S. S. Bassett, G. W. Redgrave, *et al.*, "Brain metabolite alterations and cognitive dysfunction in early huntington's disease," *Movement Disorders*, vol. 27, no. 7, pp. 895–902, 2012.

[63] C. Juchem and R. A. de Graaf, "B_0 magnetic field homogeneity and shimming for *in vivo* magnetic resonance spectroscopy," *Analytical biochemistry*, vol. 529, pp. 17–29, 2017.

[64] J. Near, A. D. Harris, C. Juchem, R. Kreis, M. Marjańska, G. Öz, J. Slotboom, M. Wilson, and C. Gasparovic, "Preprocessing, analysis and quantification in single-voxel magnetic resonance spectroscopy: experts' consensus recommendations," *NMR in Biomedicine*, vol. 34, no. 5, p. e4257, 2021.

[65] A. Lin, O. Andronesi, W. Bogner, I.-Y. Choi, E. Coello, C. Cudalbu, C. Juchem, G. J. Kemp, R. Kreis, M. Krššák, *et al.*, "Minimum reporting standards for *in vivo* magnetic resonance spectroscopy (mrsinmrs): experts' consensus recommendations," *NMR in Biomedicine*, vol. 34, no. 5, p. e4484, 2021.

[66] O. C. Andronesi, P. K. Bhattacharyya, W. Bogner, I.-Y. Choi, A. T. Hess, P. Lee, E. M. Meintjes, M. D. Tisdall, M. Zaitzev, and A. van der Kouwe, "Motion correction methods for mrs: experts' consensus recommendations," *NMR in Biomedicine*, vol. 34, no. 5, p. e4364, 2021.

[67] B. Keating, W. Deng, J. C. Roddey, N. White, A. Dale, V. A. Stenger, and T. Ernst, "Prospective motion correction for single-voxel ^{1}h-mr spectroscopy," *Magnetic resonance in medicine*, vol. 64, no. 3, pp. 672–679, 2010.

[68] M. Wilson, "Robust retrospective frequency and phase correction for single-voxel mr spectroscopy," *Magnetic resonance in medicine*, vol. 81, no. 5, pp. 2878–2886, 2019.

[69] A. D. Harris, N. A. Puts, P. B. Barker, and R. A. Edden, "Spectral-editing measurements of gaba in the human brain with and without macromolecule suppression," *Magnetic resonance in medicine*, vol. 74, no. 6, pp. 1523–1529, 2015.

[70] M. Mikkelsen, A. D. Harris, R. A. Edden, and N. A. Puts, "Macromolecule-suppressed gaba measurements correlate more strongly with behavior than macromolecule - contaminated gaba+ measurements," *Brain research*, vol. 1701, pp. 204–211, 2018.

Appendices

A

Gannet Pre-Initialise

```
function MRS_struct = GannetPreInitialise(MRS_struct)


% Acquisition parameters
     MRS_struct.p.target = {'GABAGlx'}; % edited metabolite(s) of interest;
allowable options are:
                                        % if MEGA-PRESS:
                                        %    {'GABAGlx'}, {'GSH'}, {'Lac'}, or
{'EtOH'}
                                        % if HERMES:
                                        %    {'GABAGlx','GSH'}, {'Lac','GSH'}, or
{'EtOH','GABA','GSH'}
                                        % if HERCULES:
                                        %    {'GABAGlx','GSH'}
                                        % if phantom data:
                                        %    and MEGA-PRESS: {'GABA'}, {'Glx'},
{'GSH'}, {'Lac'}, or {'EtOH'}
                                        % and HERMES: {'GABA','GSH'},
{'Glx','GSH'}, {'Lac','GSH'}, or {'EtOH','GABA','GSH'}
     MRS_struct.p.ONOFForder = 'onfirst'; % order of editing pulses; options are
'onfirst' or 'offfirst'
     MRS_struct.p.seqorig = 'JHU'; % origin of Philips patch; options are 'JHU'
or 'Philips'


% Analysis parameters
     MRS_struct.p.LB = 3; % line-broadening (in Hz)
     MRS_struct.p.water_phase_correction = 1; % 1 = YES; perform eddy current
correction on water data
     MRS_struct.p.data_phase_correction = 1; % 1 = YES; perform eddy current
correction on metabolite data
     MRS_struct.p.water_removal = 1; % 1 = YES; remove residual water signal
using HSVD
     MRS_struct.p.AlignTo = 'RobustSpecReg'; % options are 'RobustSpecReg'
(recommended), 'SpecReg', 'SpecRegHERMES',
                                             % 'Cr', 'Cho', 'NAA', 'H2O', 'CrOFF'
or 'none'
     MRS_struct.p.Vox = {'vox1','vox2'}; % for naming voxels in PRIAM data, e.g.:
{'anterior','posterior'}, {'right','left'}, etc.
     MRS_struct.p.FitResidWater = 1; % 1 = YES, fit the residual water signal in
the DIFF spectrum to calculate water suppression factor


% Flags
     MRS_struct.p.HERMES = 0; % 1 = YES, 0 = NO
     MRS_struct.p.HERCULES = 0; % 1 = YES, 0 = NO (if 1, MRS_struct.p.HERMES
*must* be set to 1 as well)
     MRS_struct.p.PRIAM = 0; % 1 = YES, 0 = NO
     MRS_struct.p.phantom = 0; % 1 = YES (assumes phantom was scanned at room
temperature), 0 = NO (for in vivo data)
     MRS_struct.p.mat = 1; % 1 = YES, save MRS_struct as .mat file
     MRS_struct.p.sdat = 0; % 1 = YES, save processed difference spectrum as
.sdat file (only for Philips SDAT MEGA-PRESS datasets)

     MRS_struct.p.csv = 1; % 1 = YES, extract useful data from MRS_struct and
export to .csv file (applies to GannetFit, GannetSegment and GannetQuantify)
end
```

```
ans =

   struct with fields:

     p: [1×1 struct]
```

Published with MATLAB® R2019a